Electron transport in disordered graphene

P. M. Ostrovsky,[1,2] I. V. Gornyi,[1,*] and A. D. Mirlin[1,3,†]
[1]*Institut für Nanotechnologie, Forschungszentrum Karlsruhe, 76021 Karlsruhe, Germany*
[2]*L. D. Landau Institute for Theoretical Physics RAS, 119334 Moscow, Russia*
[3]*Institut für Theorie der kondensierten Materie, Universität Karlsruhe, 76128 Karlsruhe, Germany*
(Received 24 September 2006; revised manuscript received 3 November 2006; published 28 December 2006)

We study the electron transport properties of a monoatomic graphite layer (graphene) with different types of disorder. We show that the transport properties of the system depend strongly on the character of disorder. Away from half filling, the concentration dependence of conductivity is linear in the case of strong scatterers, in line with recent experimental observations, and logarithmic for weak scatterers. At half filling the conductivity is of the order of e^2/h if the randomness preserves one of the chiral symmetries of the clean Hamiltonian, whereas for generic disorder the conductivity is strongly affected by localization effects.

DOI: 10.1103/PhysRevB.74.235443 PACS number(s): 73.63.−b, 73.22.−f

I. INTRODUCTION

Recently, Novoselov *et al.* have succeeded in the fabrication of monolayer graphite (graphene) samples.[1] Subsequent transport measurements[2–6] have shown that graphene is a conductor with remarkable electronic properties. These experimental discoveries have triggered an outbreak of theoretical activity; see, in particular, Refs. 7–40. Charge carriers in graphene have a relativistic (Dirac) spectrum,[41,42] which makes the transport properties of this material highly interesting from the point of view of both fundamental physics and potential applications. It is widely believed that graphene-based devices may be of outstanding importance for future nanoelectronics.

This work has been motivated by the following two experimental observations.[2,3] First, it was found that the graphene conductivity is linear in the concentration of carriers (counted from half filling) with a high accuracy. Second, it was found that at half filling the conductivity (per spin direction and per valley) is close to e^2/h and does not show any definite temperature dependence in a broad temperature range. The aim of this paper is to analyze what one should expect for conductivity from the theoretical point of view and whether these theoretical predictions may be compatible with experimental findings. We will see that, in view of the unconventional character of the graphene spectrum, the theoretical results depend crucially on the nature of disorder.

The structure of the paper is as follows. In Sec. II we introduce the model describing the electronic properties of graphene with various types of disorder. In Sec. III we analyze the dependence of conductivity on the electron concentration away from the half-filling point. We consider the two limits of weak and strong scatterers and construct the corresponding "phase diagram." Section IV is devoted to the conductivity at half filling under the assumption that the disorder preserves one of the chiral symmetries of the Dirac Hamiltonian. Our findings are summarized in Sec. V. Some technical details are presented in two appendixes.

II. THE MODEL

A. Clean graphene

The carbon atoms of graphene are arranged in a honeycomb lattice [see Fig. 1(a)] with period $a=2.46$ Å. Each carbon atom of intrinsic graphene has one valence electron forming π bonds to three neighbors. The electronic spectrum of graphene is well described by the tight-binding model[41] taking into account the nearest-neighbor hopping. The first Brillouin zone for this system has the form of a hexagon [see Fig. 1(b)] with the distance $k_0=2h/3a$ from the center to the apex. The honeycomb lattice contains two sites per elementary cell. This permits grouping all the atoms into two sublattices A and B. The nearest neighbors of an atom from sublattice A belong to sublattice B and vice versa. The symmetry group of the honeycomb lattice contains an element swapping the two sublattices. Hence, for each value of the quasimomentum $\mathbf{k}$ within the Brillouin zone, two states exist with energies $\pm E(\mathbf{k})$. These two spectrum branches are degenerate at isolated points in the corners of the Brillouin zone, $E(\mathbf{k}_0)=0$. With one electron per site the system is exactly in the half-filling state when the nodal points of the spectrum lie at the Fermi level. Among six apices of the hexagonal Brillouin zone only two are nonequivalent. They are referred to as K and K'. The electrons with momentum close to these two points, and hence with low energy, are relevant in studying the physics of the system for electron concentrations not too far from half filling.

The tight-binding Hamiltonian is a 4×4 matrix operating in the AB space of the two sublattices and in the K–K' space of the valleys. Therefore we introduce the four-component wave function

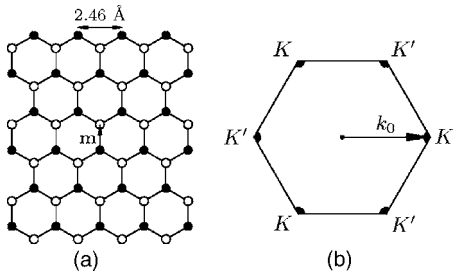

FIG. 1. (a) Honeycomb lattice of the carbon atoms of graphene. Solid and open circles denote the atoms of A and B sublattices, respectively. (b) The first Brillouin zone of graphene. The nodal points of the spectrum are located in the corners of the zone. The two nonequivalent nodal points are denoted as K and K'.

$$\Psi = \{\phi_{AK}, \phi_{BK}, \phi_{BK'}, \phi_{AK'}\}^T. \quad (1)$$

In this representation the Hamiltonian has the form (hereafter we assume $\hbar = 1$)

$$H = v_0 \tau_3 \boldsymbol{\sigma} \cdot \mathbf{k}. \quad (2)$$

Here τ_3 is the third Pauli matrix in the K-K' space and $\boldsymbol{\sigma} = \{\sigma_1, \sigma_2\}$ is the two-dimensional vector of Pauli matrices in the AB space. The Fermi velocity in graphene is $v_0 \simeq 10^8$ cm/s. In fact, the form of the Hamiltonian (2) is universal and does not rely on the tight-binding approximation. The degeneracy of the spectrum in K and K' points is provided by the two-dimensional representation of the honeycomb lattice symmetry group while the expression (2) is the first-order k expansion near these points. As k is increased the higher-order nonuniversal terms of this expansion come into play. For our purposes, it will be sufficient to introduce the high-energy cutoff Δ and to assume the spectrum to be linear up to $|\mathbf{k}| = \Delta / v_0$. Indeed, all divergent momentum integrals appearing below have logarithmic character; thus, details of the high-energy regularization are irrelevant. The Green function for the Hamiltonian (2) of clean graphene reads

$$G_0^{R(A)}(\varepsilon, \mathbf{k}) = \frac{\varepsilon + v_0 \tau_3 \boldsymbol{\sigma} \cdot \mathbf{k}}{(\varepsilon \pm i0)^2 - v_0^2 k^2}. \quad (3)$$

B. Potential disorder

We incorporate now disorder in the model. Let us consider first the impurities modifying the potential on nearby lattice sites. A detailed description due to McCann and Fal'ko[7] contains ten real parameters for the potential of a single impurity. In the present paper we will use the simplified model introduced by Shon and Ando in Ref. 43, which retains the essential physics of the problem. This model treats impurities in the framework of the same tight-binding approximation as was used for the pure system. An impurity is placed at a site of the lattice and has a potential $U(\mathbf{r})$. We use the two discrete Fourier transforms of this function with respect to the two sublattices.

$$U_{\mathbf{q}} = \frac{\sqrt{3}a^2}{2} \sum_{\mathbf{r}} U(\mathbf{r}) e^{-i\mathbf{q}\cdot\mathbf{r}}, \quad (4)$$

$$U'_{\mathbf{q}} = \frac{\sqrt{3}a^2}{2} \sum_{\mathbf{r}} U(\mathbf{r} - \mathbf{m}) e^{-i\mathbf{q}\cdot\mathbf{r}}. \quad (5)$$

The summation runs over all elementary cells of the honeycomb lattice, and the vector $\mathbf{m}$ points from the A sublattice site to the B sublattice site of the same elementary cell [see Fig. 1(a)]. The quantity $U_{\mathbf{q}}$ is the scattering amplitude for electrons of the same sublattice where the impurity resides, while $U'_{\mathbf{q}}$ is the scattering amplitude for electrons of the other sublattice.

Assuming $U_{\mathbf{q}}$ and $U'_{\mathbf{q}}$ are slow functions of the momentum $\mathbf{q}$, we keep only two values of these amplitudes for intravalley, U_0 and U'_0, and intervalley, U_{k_0} and U'_{k_0}, scattering. The hexagonal symmetry of the honeycomb lattice makes the amplitude U'_{k_0} vanish while the three other amplitudes are real. Thus we are left with the three parameters of an impurity potential. It is straightforward to put them in a matrix in the four-dimensional representation (1). If the impurity site belongs to sublattice A and to the elementary cell $\mathbf{r}_i$, the scattering matrix takes the form

$$V_{\mathbf{q}}^{\mathrm{A}}(\mathbf{r}_i) = \begin{pmatrix} U_0 & 0 & 0 & U_{k_0} e^{-2i\mathbf{k}_0\cdot\mathbf{r}_i} \\ 0 & U'_0 & 0 & 0 \\ 0 & 0 & U'_0 & 0 \\ U_{k_0} e^{2i\mathbf{k}_0\cdot\mathbf{r}_i} & 0 & 0 & U_0 \end{pmatrix} e^{-i\mathbf{q}\cdot\mathbf{r}_i}. \quad (6)$$

For the impurity located in the sublattice B, we have

$$V_{\mathbf{q}}^{\mathrm{B}}(\mathbf{r}_i) = \begin{pmatrix} U'_0 & 0 & 0 & 0 \\ 0 & U_0 & U_{k_0} e^{-2i\mathbf{k}_0\cdot\mathbf{r}_i} & 0 \\ 0 & U_{k_0} e^{2i\mathbf{k}_0\cdot\mathbf{r}_i} & U_0 & 0 \\ 0 & 0 & 0 & U'_0 \end{pmatrix} e^{-i\mathbf{q}\cdot\mathbf{r}_i}. \quad (7)$$

If the potential disorder is weak and obeys a Gaussian distribution, the only relevant quantity is the autocorrelation function of the second order $\langle V_{\mathbf{q}} \otimes V_{-\mathbf{q}} \rangle$. We denote the impurity concentration by n_{imp} and obtain after averaging with respect to positions of the impurities

$$\begin{aligned} \langle V_{\mathbf{q}} \otimes V_{-\mathbf{q}} \rangle &= \frac{n_{\mathrm{imp}}}{2} \langle V_{\mathbf{q}}^{\mathrm{A}}(\mathbf{r}_i) \otimes V_{-\mathbf{q}}^{\mathrm{A}}(\mathbf{r}_i) + V_{\mathbf{q}}^{\mathrm{B}}(\mathbf{r}_i) \otimes V_{-\mathbf{q}}^{\mathrm{B}}(\mathbf{r}_i) \rangle \\ &= 2\pi v_0^2 \Big\{ \alpha_0 \sigma_0 \tau_0 \otimes \sigma_0 \tau_0 + \gamma_z \sigma_3 \tau_3 \otimes \sigma_3 \tau_3 \\ &\quad + \frac{\beta_\perp}{4} [\sigma_1 \tau_1 \otimes \sigma_1 \tau_1 + \sigma_1 \tau_2 \otimes \sigma_1 \tau_2 + \sigma_2 \tau_1 \\ &\quad \otimes \sigma_2 \tau_1 + \sigma_2 \tau_2 \otimes \sigma_2 \tau_2] \Big\}. \end{aligned} \quad (8)$$

Here we introduce the three dimensionless parameters

$$\alpha_0 = \frac{n_{\mathrm{imp}}}{8\pi v_0^2} (U_0 + U'_0)^2, \quad (9a)$$

$$\gamma_z = \frac{n_{\mathrm{imp}}}{8\pi v_0^2} (U_0 - U'_0)^2, \quad (9b)$$

$$\beta_\perp = \frac{n_{\mathrm{imp}}}{4\pi v_0^2} U_{k_0}^2. \quad (9c)$$

While the notations in Eqs. (9) may seem strange at this stage, they will be explained later when we consider randomness of a broader class. To further simplify the calculations, we will concentrate on the two limiting cases of short- and long-range potential disorder.[43]

The *short-range* impurity scatters electrons in the same sublattice only. It is equivalent to a potential shift at a particular lattice site. The amplitudes are $U_0 = U_{k_0} = U/2$ and $U'_0 = 0$. Thus we are left with a single parameter U. The parameters, Eqs. (9), obey the relation $\alpha_0 = \gamma_z = \beta_\perp / 2$.

The *long-range* impurity scatters electrons in both sublattices equally but only within one valley. The scattering length is large in comparison with the lattice constant but is still smaller than the Fermi wavelength. The amplitudes are $U_0=U_0'=U$ and $U_{k_0}=0$. We have again the single parameter U as in the case of short-range disorder. Among the parameters (9) only α_0 is not zero in this case.

It is worth emphasizing that throughout the paper we consider a macroscopically homogeneous system (i.e., assume that the disorder range is small compared to the transport mean free path). Slow spatial variations of the chemical potential might be important (especially in the vicinity of the Dirac point) in realistic structures, depending on technological details. In any case, the analysis of the transport in a macroscopically homogeneous system—which is the subject of the present work—should be done first, in order to find the microscopic conductivity. This result can serve as a starting point for the study of the macroscopically inhomogeneous systems.

C. Generic disorder and chiral symmetries

Let us turn now to the analysis of the symmetries of the clean graphene Hamiltonian (2). First, the system is obviously uniform and isotropic. Any disorder considered in this paper preserves these symmetries on average, so we do not pay much attention to them here. Second, due to the two valley structure of the electron spectrum, the whole SU(2) symmetry group exists in an *isospin* space of the valleys. The generators of this group are[26]

$$\Lambda_x=\sigma_3\tau_1,\quad \Lambda_y=\sigma_3\tau_2,\quad \Lambda_z=\sigma_0\tau_3. \tag{10}$$

These three operators commute with the Hamiltonian and anticommute with each other. There are other three matrices $\Sigma_{x,y,z}$ introduced in Ref. 26:

$$\Sigma_x=\sigma_1\tau_3,\quad \Sigma_y=\sigma_2\tau_3,\quad \Sigma_z=\sigma_3\tau_0. \tag{11}$$

These operators generate an additional SU(2) group of a *pseudospin*. They *do not* commute with the Hamiltonian (2); however, any of these matrices commute with any of $\Lambda_{x,y,z}$.

Third, the time inversion operation (we denote it T_0) in the representation (1) reads

$$T_0:\ A\mapsto \sigma_1\tau_1A^T\sigma_1\tau_1. \tag{12a}$$

The Hamiltonian (2) is invariant under time inversion (note that the momentum operator changes sign under transposition). Combining the T_0 operation with any of $\Lambda_{x,y,z}$ from Eq. (10) we produce three additional symmetry operations

$$T_x:\ A\mapsto \sigma_2\tau_0A^T\sigma_2\tau_0, \tag{12b}$$

$$T_y:\ A\mapsto \sigma_2\tau_3A^T\sigma_2\tau_3, \tag{12c}$$

$$T_z:\ A\mapsto \sigma_1\tau_2A^T\sigma_1\tau_2. \tag{12d}$$

Finally, there is one more—namely, *chiral*—symmetry C_0 and its three counterparts generated by simultaneous application of C_0 and $\Lambda_{x,y,z}$:

$$C_0:\ A\mapsto -\sigma_3\tau_0A\sigma_3\tau_0, \tag{13a}$$

$$C_x:\ A\mapsto -\sigma_0\tau_1A\sigma_0\tau_1, \tag{13b}$$

$$C_y:\ A\mapsto -\sigma_0\tau_2A\sigma_0\tau_2, \tag{13c}$$

$$C_z:\ A\mapsto -\sigma_3\tau_3A\sigma_3\tau_3. \tag{13d}$$

The chiral symmetry C_0 can be viewed as the basic chiral symmetry of the Hamiltonian (2). Indeed, C_0 is distinguished by the fact that it is directly produced by the Hamiltonian (2) as $i\sigma_3\tau_0=v_0^{-2}(\partial H/\partial k_x)(\partial H/\partial k_y)$, while other chiral symmetries require a rotation in the isospin space.

Generally, the chiral symmetry implies that the Hamiltonian takes block-off-diagonal form under a proper unitary transformation. A generic disorder preserving C_z symmetry can have only *off-diagonal* matrix elements in the AB space of sublattices. Some specific examples of chiral symmetry are (i) bond disorder due to distortions of the lattice (C_z symmetry), (ii) random magnetic field (all four symmetries $C_{0,x,y,z}$), (iii) dislocations, which are equivalent to a random non-Abelian gauge field[14,44] (C_0), and (iv) infinitely strong short-range on-site impurities (C_z). In the latter case an electron cannot occupy the impurity site, implying that all the bonds adjacent to the impurity are effectively cut. Any potential disorder other than the described extreme case violates all chiral symmetries. The symmetry is also broken by a nonzero chemical potential. Thus the impact of the chiral character of disorder will be particularly important at the degeneracy point $\varepsilon=0$. In Sec. IV we consider various effects of chiral symmetry on the density of states and conductivity of graphene.

The average isotropy of the disordered graphene implies that Λ_x and Λ_y symmetries of the Hamiltonian are present or absent simultaneously. Below we combine them into a single notation $\Lambda_\perp$ and proceed in the same way with $T_\perp$ and $C_\perp$. In Table I we list all possible matrix structures of the disorder [in the representation defined by Eq. (1)] along with their symmetries. There are nine different structures altogether.[26] Those five of them that do not violate time inversion symmetry coincide[46] with ones considered by Aleiner and Efetov.[32] We also give the notations of Ref. 45, where the disordered Dirac Hamiltonian obeying C_z chiral symmetry was considered.

III. CONDUCTIVITY FAR FROM THE DEGENERACY POINT

In this section, we will study the concentration dependence of the conductivity far from half filling, when the size of Fermi circles around K and K' points is large in comparison with the inverse mean free path. The dimensionless Drude conductivity (measured in units of e^2/h) is then large,[43] so that, at realistic temperatures, one can neglect as a first approximation the quantum corrections related to localization. As a starting point, we will employ the *self-consistent T-matrix approximation*[47] (SCTMA), which takes into account all orders of scattering at an impurity. It will allow us to study the whole "phase diagram" including the limits of weak (Born) and strong (unitary) scatterers and the crossover between them. We will discuss the status of the

TABLE I. The symmetries of various disorders in graphene. The first five rows of the table contain disorders preserving time-inversion symmetry. They were considered in Ref. 32. The next four rows are occupied by disorders violating time-inversion symmetry. We present the matrix structure of the disorder in two forms: by matrices $\sigma_i\tau_j$ and by matrices $\Sigma_i\Lambda_j$ as in Ref. 26. The notations we use for the amplitudes of the disorder in Gaussian limit are listed in the third column; a rigorous definition of these parameters can be found in Appendix A. The letters α, β, and γ correspond to Λ_0, $\Lambda_{x,y}$, and Λ_z components of the disorder Hamiltonian, respectively, while the subscripts 0, $\perp$, and z indicate the structure in the Σ space. In the fourth and fifth columns we give alternative notations from Refs. 32 and 45. Our notations are close to those of Ref. 32; the only difference is in the case of a fully diagonal potential: our parameter α_0 corresponds to γ_0 from Ref. 32, while we use γ_0 for the disorder $\sigma_0\tau_3$ discriminating the two valleys.

Disorder structure		Disorder strength			Hamiltonian symmetries							
$\sigma_i\tau_j$	$\Sigma_i\Lambda_j$	This paper	Ref. 32	Ref. 45	$\Lambda_\perp$	Λ_z	T_0	$T_\perp$	T_z	C_0	$C_\perp$	C_z
$\sigma_0\tau_0$	$\Sigma_0\Lambda_0$	α_0	$\gamma_0/2\pi v^2$		+	+	+	+	+	−	−	−
$\sigma_{\{1,2\}}\tau_{\{1,2\}}$	$\Sigma_{\{x,y\}}\Lambda_{\{x,y\}}$	$\beta_\perp$	$2\beta_\perp/\pi v^2$		−	−	+	−	−	+	−	−
$\sigma_{1,2}\tau_0$	$\Sigma_{x,y}\Lambda_z$	$\gamma_\perp$	$\gamma_\perp/\pi v^2$	g_A	−	+	+	−	+	+	−	+
$\sigma_0\tau_{1,2}$	$\Sigma_z\Lambda_{x,y}$	β_z	$\beta_z/\pi v^2$	$\sqrt{2}g_m$	−	−	+	−	−	−	−	+
$\sigma_3\tau_3$	$\Sigma_z\Lambda_z$	γ_z	$\gamma_z/2\pi v^2$		−	+	+	−	+	−	+	−
$\sigma_3\tau_{1,2}$	$\Sigma_0\Lambda_{x,y}$	β_0		$\sqrt{2}g_\mu$	−	−	−	−	+	−	−	+
$\sigma_0\tau_3$	$\Sigma_0\Lambda_z$	γ_0			−	+	−	+	−	−	+	−
$\sigma_{1,2}\tau_3$	$\Sigma_{x,y}\Lambda_0$	$\alpha_\perp$		$g_{A'}$	+	+	−	−	−	+	+	+
$\sigma_3\tau_0$	$\Sigma_z\Lambda_0$	α_z			+	+	−	−	−	−	−	−

SCTMA in Sec. III B, where we will show that while it is not quantitatively justified in the Born regime, it yields a qualitatively correct behavior of the conductivity far from the degeneracy point.

A. Self-consistent T-matrix approximation

1. Potential disorder

Let us first consider the disorder induced by randomly located impurities which create the potential given by Eqs. (6) and (7). The sum of all scattering orders determines the complete impurity's T matrix, as represented graphically in Fig. 2. Averaging the T matrix with respect to the position of the impurity, we find

$$\langle T(\varepsilon)\rangle = \frac{1}{4}\left[\frac{2U_0'}{1-U_0'g} + \frac{U_0+U_{k_0}}{1-(U_0+U_{k_0})g} + \frac{U_0-U_{k_0}}{1-(U_0-U_{k_0})g}\right], \tag{14}$$

with g being the integral of the Green function,

$$g(\varepsilon) = \int \frac{d^2k}{(2\pi)^2} G(\varepsilon,\mathbf{k}). \tag{15}$$

This quantity has trivial matrix structure due to the angular integration. The electron's self-energy is determined by the average value of the T matrix, Eq. (14):

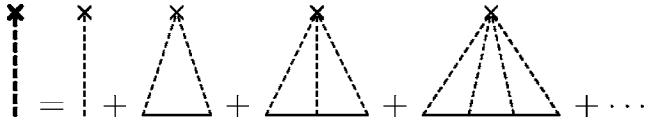

FIG. 2. Graphical representation of the T matrix describing the electron scattering off an impurity.

$$\Sigma(\varepsilon) = n_{\text{imp}}\langle T(\varepsilon)\rangle, \tag{16}$$

where n_{imp} is the concentration of impurities.

Inserting Eq. (16) into the bare Green function (3),

$$G(\varepsilon,\mathbf{k}) = \frac{\varepsilon-\Sigma(\varepsilon)+v_0\tau_3\boldsymbol{\sigma}\mathbf{k}}{[\varepsilon-\Sigma(\varepsilon)]^2-v_0^2k^2}, \tag{17}$$

and calculating the momentum integral in Eq. (15), we get

$$g(\varepsilon) = -\frac{\varepsilon-\Sigma(\varepsilon)}{4\pi v_0^2}\ln\frac{-\Delta^2}{[\varepsilon-\Sigma(\varepsilon)]^2}. \tag{18}$$

The logarithmic divergence is cut at the momentum Δ/v_0. The sign of the imaginary part of $g(\varepsilon)$, and hence of the self-energy, is determined by the type of Green function (advanced or retarded) we are considering.

Equations (14), (16), and (18) form a closed set that self-consistently determines the self-energy $\Sigma(\varepsilon)$. These equations take into account all the diagrams with nonintersecting impurity lines. In the two extreme cases of short- and long-range potential impurities the self-consistency equation reduces to the form

$$\Sigma(\varepsilon) = \begin{cases} \dfrac{n_{\text{imp}}U}{1-Ug(\varepsilon)}, & \text{long range,} \\ \dfrac{n_{\text{imp}}U}{4[1-Ug(\varepsilon)]}, & \text{short range.} \end{cases} \tag{19}$$

Once these equations are solved, one can find the density of states and the conductivity of the system. The density of states (per one spin component) is

FIG. 3. Diagrams for the Drude conductivity including the vertex correction.

$$\rho(\varepsilon) = -\frac{1}{\pi}\,\mathrm{Im\,Tr}\int \frac{d^2k}{(2\pi)^2} G^R(\varepsilon,\mathbf{k}) = -\frac{4}{\pi}\,\mathrm{Im}\, g^R(\varepsilon). \tag{20}$$

The conductivity at zero frequency and wave vector is given by the Kubo formula

$$\sigma^{\alpha\beta}(\varepsilon) = \frac{2}{\pi}\int d^2(r-r') \times \mathrm{Tr}\langle j^\alpha \mathrm{Im}\, G^R(\varepsilon;\mathbf{r},\mathbf{r}') j^\beta \,\mathrm{Im}\, G^R(\varepsilon;\mathbf{r}',\mathbf{r})\rangle. \tag{21}$$

Due to the linear dependence of the Hamiltonian on $\mathbf{k}$, the current operator is independent of the momentum,

$$\mathbf{j} = e\frac{\partial H}{\partial \mathbf{k}} = ev_0\tau_3\boldsymbol{\sigma}. \tag{22}$$

This results in the absence of the diamagnetic term in the expression for conductivity.

Equation (21) includes averages of the type $\langle jG^R jG^A\rangle$ along with $\langle jG^R jG^R\rangle$ and $\langle jG^A jG^A\rangle$. The first one is large in the metallic regime when the energy ε is far from the degeneracy point, while the two others give a contribution of the order of conductance quantum e^2/h. Therefore we will neglect those two in this section.

As discussed above, we will use the Drude approximation for the conductivity, neglecting weak localization corrections. Graphically, this is equivalent to the summation of the diagrams shown in Fig. 3. Due to the vector nature of the current operator in the vertex, only the diagonal parts of the Green functions contribute to the result. We introduce the notation

$$\Pi^{RA}(\varepsilon) = \int \frac{d^2k}{(2\pi)^2}\,\mathrm{diag}G^R(\varepsilon,\mathbf{k})\mathrm{diag}G^A(\varepsilon,\mathbf{k}). \tag{23}$$

The sum of the ladder diagrams in Fig. 3 gives the correction to the current vertex. We will use a special notation $\mathcal{V}$ for this vertex correction factor. In the limit of the short-range potential disorder, we have $\mathcal{V}=1$. In the opposite long-range case, the summation of ladder diagrams yields

$$\mathcal{V} = \frac{1}{1-\dfrac{n_{\mathrm{imp}}U^2}{|1-Ug|^2}\Pi^{RA}}. \tag{24}$$

The resulting Drude conductivity has the form

$$\sigma(\varepsilon) = \frac{4}{\pi}e^2v_0^2\mathcal{V}\Pi^{RA}. \tag{25}$$

In the following sections we will solve the self-consistency equations and find the density of states and the conductivity in various limits. We will also analyze the corrections to the SCTMA coming from diagrams with intersecting disorder lines.

2. Generic Gaussian disorder

In the case of generic weak disorder, one can use a more general equation for the self-energy taking into account all possible disorder amplitudes (listed in Table I) in the framework of the Born approximation,

$$\Sigma(\varepsilon) = 2\pi v_0^2 \alpha g(\varepsilon). \tag{26}$$

Here α is the total strength of the disorder—-i.e., the sum of all amplitudes from Table I,

$$\alpha = \alpha_0 + \beta_0 + \gamma_0 + \alpha_\perp + \beta_\perp + \gamma_\perp + \alpha_z + \beta_z + \gamma_z. \tag{27}$$

This quantity is relevant for thermodynamic properties of the system with Gaussian disorder. The vertex correction is given by

$$\mathcal{V} = \frac{1}{1-4\pi v_0^2(\alpha-\alpha_{\mathrm{tr}})\Pi^{RA}}, \tag{28}$$

where

$$\alpha_{\mathrm{tr}} = \frac{1}{2}(\alpha_0+\beta_0+\gamma_0) + \alpha_\perp + \beta_\perp + \gamma_\perp + \frac{3}{2}(\alpha_z+\beta_z+\gamma_z). \tag{29}$$

As will be seen below [Eq. (37)], α_{tr} governs the transport properties of the Gaussian-disordered system.

Using Eqs. (9), (27), and (29), we get for weak long-range and short-range potential disorder considered above in Sec. III A 1

$$\alpha = 2\alpha_{\mathrm{tr}} = \frac{n_{\mathrm{imp}}U^2}{2\pi v_0^2}, \quad \text{long range}, \tag{30}$$

$$\alpha = \alpha_{\mathrm{tr}} = \frac{n_{\mathrm{imp}}U^2}{8\pi v_0^2}, \quad \text{short range}. \tag{31}$$

B. Born limit: Weak scatterers

1. Self-consistent Born approximation

The simplest situation is the Born limit of weak scattering. Only the lowest scattering order is relevant in this case. This yields the *self-consistent Born approximation* (SCBA),[43,56,57] Eq. (26). In this limit, we deal with a generic weak disorder described by all nine parameters listed in Table I. The results for the special case of potential disorder are easily restored from the general results with the help of Eqs. (9).

The SCBA equation has the form

$$\Sigma(\varepsilon) = -\frac{\alpha}{2}[\varepsilon-\Sigma(\varepsilon)]\ln\frac{-\Delta^2}{[\varepsilon-\Sigma(\varepsilon)]^2}. \tag{32}$$

This equation was studied numerically by Shon and Ando in Ref. 43; we treat it below by analytical means.

Weak disorder introduces an exponentially small energy scale

$$\Gamma_0 = \Delta e^{-1/\alpha}. \tag{33}$$

At large energies $\varepsilon \gg \Gamma_0$, we solve Eq. (32) by iterations, while at low energies the solution is found in the form of a series in powers of ε. The resulting self energy is[61] (upper sign, retarded; lower sign, advanced)

$$\Sigma(\varepsilon) = \begin{cases} \mp i\Gamma_0 - \dfrac{\varepsilon}{\alpha}, & |\varepsilon| \ll \Gamma_0, \\ -\alpha\varepsilon \ln\dfrac{\Delta}{|\varepsilon|} \mp \dfrac{i\pi\alpha|\varepsilon|}{2}\left[1 + 2\alpha \ln\dfrac{\Delta}{|\varepsilon|}\right], & |\varepsilon| \gg \Gamma_0. \end{cases} \tag{34}$$

Substituting Eq. (34) into Eq. (20), we get the density of states

$$\rho_{\mathrm{SCBA}}(\varepsilon) = \frac{2|\mathrm{Im}\Sigma(\varepsilon)|}{\pi^2 v_0^2 \alpha} = \begin{cases} \dfrac{2\Gamma_0}{\pi^2 v_0^2 \alpha}, & \varepsilon \ll \Gamma_0, \\ \dfrac{|\varepsilon|}{\pi v_0^2}\left[1 + 2\alpha \ln\dfrac{\Delta}{|\varepsilon|}\right], & \varepsilon \gg \Gamma_0. \end{cases} \tag{35}$$

At high energies the found density of states is close to its value in clean graphene, $\rho_0(\varepsilon) = |\varepsilon|/\pi v_0^2$.

To evaluate the SCBA conductivity, we first find the polarization operator (23),

$$\Pi^{RA}(\varepsilon) = \frac{1}{4\pi v_0^2 \alpha} \frac{\varepsilon}{\varepsilon - \mathrm{Re}\,\Sigma(\varepsilon)}. \tag{36}$$

With the help of Eqs. (25) and (24) we find the general expression for the SCBA conductivity:

$$\sigma_{\mathrm{SCBA}}(\varepsilon) = \frac{e^2}{\pi^2}\left[\frac{\varepsilon}{\alpha_{\mathrm{tr}}\varepsilon - \alpha\,\mathrm{Re}\,\Sigma(\varepsilon)} + 1\right]. \tag{37}$$

Here the first term comes from the retarded-advanced (RA) sector whereas the second term (unity) is the contribution of RR and AA correlators. At high energies ($\varepsilon \gg \Gamma_0$) the SCBA conductivity is governed by the RA term and takes the form

$$\sigma_{\mathrm{SCBA}}(\varepsilon) \simeq \frac{e^2}{\pi^2 \alpha_{\mathrm{tr}}}\left[1 - \frac{\alpha^2}{\alpha_{\mathrm{tr}}} \ln\frac{\Delta}{|\varepsilon|}\right]. \tag{38}$$

The found conductivity shows a logarithmic energy dependence above an exponentially small energy scale. At half filling $\varepsilon \ll \Gamma_0$, the SCBA yields $\sigma_{\mathrm{SCBA}} = 2e^2/\pi^2\hbar$. This value of conductivity includes contributions of the form $\langle jG^R jG^R\rangle$ and $\langle jG^A jG^A\rangle$, which were discarded at $\varepsilon \gg \Gamma_0$. A conductivity value of the order of e^2/h does not make much sense in the present context, in view of the localization effects. We will return to this issue in Sec. IV.

2. Logarithmic corrections and renormalization group

The leading term in the Drude conductivity (37) is proportional to $\alpha_{\mathrm{tr}}^{-1}$ and is independent of energy. The SCBA gives also a logarithmic correction, which is small at large energies. There exist, however, other contributions of the same order that are not included in the SCBA calculation; see Fig. 4. An efficient tool for resummation of the logarithmic contributions in all orders is the renormalization group (RG). For the case of two-dimensional (2D) Dirac fermions subjected to various types of disorder it was developed by Dotsenko and Dotsenko[62] for the random bond Ising model, by Ludwig *et al.*[63] in the context of the quantum Hall effect, and by Nersesyan *et al.*[64] and Bocquet *et al.*[65] in application to dirty superconductors with unconventional pairing (see also the review by Altland *et al.*[66]), as well as by Guruswamy *et al.*[45] for a model with chiral disorder (C_z in our notation). Very recently, Aleiner and Efetov[32] returned to such a RG in the context of disordered graphene. The renormalization of the conductivity gives rise to its dependence on energy (or, equivalently, on the electronic concentration; see below).

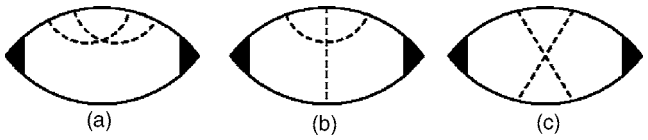

FIG. 4. Diagrams yielding logarithmic corrections to the conductivity not included in the SCBA.

Let us briefly analyze the leading logarithmic corrections and the RG results and compare them to the SCBA in the simplest case of diagonal disorder with the only parameter $\alpha = 2\alpha_{\mathrm{tr}} = \alpha_0$ (see Table I). The diagrams of Fig. 4 give logarithmic corrections proportional to $\alpha_0 \ln(\Delta/|\varepsilon|)$ and missed by the SCBA:

$$\delta\sigma = \frac{2e^2}{\pi^2\alpha_0} \times \begin{cases} +2\alpha_0 \ln(\Delta/|\varepsilon|) & \text{(a)}, \\ -2\alpha_0 \ln(\Delta/|\varepsilon|) & \text{(b)}. \end{cases} \tag{39}$$

A contribution from diagram (c), which is potentially of the same order, vanishes after the angular integration. Since the two contributions in Eq. (39) cancel each other, the SCBA turns out to give the leading logarithmic correction even with a correct numerical coefficient,

$$\sigma(\varepsilon) = \frac{2e^2}{\pi^2\alpha_0}\left[1 - 2\alpha_0 \ln\frac{\Delta}{|\varepsilon|} + \cdots\right]. \tag{40}$$

This coincidence in the numerical coefficient seems to be accidental, however. If one takes into account disorder amplitudes other than α_0, the numerical coefficient in front of the leading logarithmic correction in SCBA [Eq. (38)] becomes in general different from the correct one (given by RG).

With lowering energy, consideration of the first-order logarithmic correction (40) becomes insufficient. As have been already mentioned, all logarithmic corrections to the density of states and conductivity can be summed up with the help of the RG.[32,45,62–66] Below we briefly present the results in the simplest case of long-range Gaussian disorder. For short-range disorder, the consideration is similar but five running couplings (first five in Table I) should be taken into account. As found in Ref. 32, this does not affect qualitatively the behavior of the conductivity.

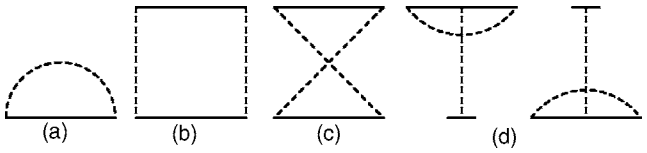

FIG. 5. One-loop RG diagrams responsible for the renormalization of (a) the energy and (b), (c), (d) the disorder couplings.

After the disorder averaging, the action for electrons in graphene with long-range disorder reads (for a generic disorder the action is given in Appendix A)

$$S[\psi] = \int d^2r[i\bar{\psi}(\varepsilon + iv_0\tau_3\boldsymbol{\sigma}\cdot\nabla - i0\Lambda)\psi + \pi v_0^2\alpha_0(\bar{\psi}\psi)^2]. \tag{41}$$

The vector superfield ψ contains $4\times2\times2=16$ components: the four-dimensional structure of the one-particle Hamiltonian is complemented by the advanced-retarded (AR) and the supersymmetric (boson-fermion) structures. The latter serves to perform the disorder averaging; alternatively, one can use the replica trick. Further, Λ is the third Pauli matrix in the AR space and the conjugated field is $\bar{\psi}=\psi^+\Lambda$. Under renormalization, the energy and the disorder strength become running couplings, $\tilde{\varepsilon}=\varepsilon(L)$ and $\tilde{\alpha}_0=\alpha_0(L)$, where L is the running ultraviolet cutoff length (measured in units of v_0/Δ). As usual, after elimination of large momenta, the real-space coordinates are rescaled to maintain the ultraviolet cutoff v_0/Δ. The coefficient v_0 of the kinetic term is kept fixed by the field renormalization (absent in the one-loop order considered below). The relevant one-loop diagrams are shown in Fig. 5 [the first two diagrams renormalizing α_0—namely, (b) and (c)—cancel exactly if the disorder is long-range]; the resulting RG equations read

$$\frac{d\tilde{\alpha}_0}{d\ln L} = 2\tilde{\alpha}_0^2, \tag{42}$$

$$\frac{d\tilde{\varepsilon}}{d\ln L} = (1+\tilde{\alpha}_0)\tilde{\varepsilon}. \tag{43}$$

Note that these equations are different from those for the random mass problem[62,63,65] only by a sign in Eq. (42). The RG equation (42) for the random scalar potential problem can be found, e.g., in Ref. 64.

Solving these differential equations, we get

$$\tilde{\alpha}_0 = \frac{\alpha_0}{1-2\alpha_0\ln L}, \tag{44}$$

$$\tilde{\varepsilon} = \frac{\varepsilon L}{\sqrt{1-2\alpha_0\ln L}}. \tag{45}$$

The renormalization proceeds until the renormalized energy $\tilde{\varepsilon}$ reaches the value of the cutoff Δ. Using this condition, we find the value of L at which the RG stops,

$$L = \frac{\Delta}{|\varepsilon|}\sqrt{1-2\alpha_0\ln\frac{\Delta}{|\varepsilon|}}. \tag{46}$$

The density of states ρ scales as $\varepsilon^{-1}L^2$—i.e., $\tilde{\rho}\tilde{\varepsilon}L^{-2}=\rho\varepsilon$. Thus, according to Eq. (45), its renormalized value $\tilde{\rho}$ is

$$\tilde{\rho} = \rho L\sqrt{1-2\alpha_0\ln L}. \tag{47}$$

At the end point of the RG we have $\tilde{\rho}=\Delta/\pi v_0^2$. Extracting ρ from Eq. (47) and substituting L from Eq. (46), we find the density of states

$$\rho(\varepsilon) = \frac{|\varepsilon|}{\pi v_0^2}\left[1-2\alpha_0\ln\frac{\Delta}{|\varepsilon|}\right]^{-1}. \tag{48}$$

Further, the conductivity is determined[67] by the renormalized dimensionless strength of the disorder $\tilde{\alpha}_0$,

$$\sigma(\varepsilon) = \frac{2e^2}{\pi^2\tilde{\alpha}_0} = \frac{2e^2}{\pi^2\alpha_0}\left[1-2\alpha_0\ln\frac{\Delta}{|\varepsilon|}\right], \tag{49}$$

in agreement with Ref. 32.

We see that the result of the SCBA, Sec. III B 1, agrees qualitatively with the fully controllable (RG) solution: the conductivity decreases logarithmically up to an exponentially small scale. The SCBA fails, however, to give a correct numerical coefficient in the exponent of Eq. (33); the correct low-energy scale Γ is

$$\Gamma = \Delta e^{-1/2\alpha_0}. \tag{50}$$

Below this new energy scale, the density of states saturates at a finite value and the Drude conductivity (with localization effects discarded) is of the order of e^2/h. Both these important features are correctly reproduced by the SCBA.

In the experiment, one changes the chemical potential μ by varying the gate voltage V_g. The electron concentration n_e is proportional to V_g, $en_e=CV_g$, where C is the corresponding capacitance per unit area. Therefore, the experimentally measured dependence $\sigma(V_g)$ is essentially $\sigma(n_e)$, up to a simple rescaling. To compare the theory with the experiment, we find the density

$$n_e(\mu) = 2\int_0^\mu d\varepsilon\rho(\varepsilon) \simeq \frac{\mu|\mu|}{\pi v_0^2}\frac{1}{1-2\alpha_0\ln(\Delta/|\mu|)}. \tag{51}$$

Combining this with Eq. (49), we get

$$\sigma(n_e) = \frac{2e^2}{\pi^2\alpha_0}\left(1-\alpha_0\ln\frac{\Delta^2}{v_0^2|n_e|}\right). \tag{52}$$

We see that the dependence of conductivity on electron density is only logarithmic, which should be contrasted with a much stronger, approximately linear, dependence observed in the experiments.[2,3] As we will see in Sec. III C, such a strong dependence does arise theoretically in the limit of strong scatterers.

One can use a more general RG approach in the case of generic Gaussian disorder when all nine parameters from Table I are nonzero. In doing so, one has to calculate the diagrams from Fig. 5 with all possible matrices at the vertices of impurity lines. The full set of one-loop perturbative RG equations can be found in Appendix A.

3. Weak localization correction

We note that the conductivity calculated above is not the total conductivity far from the degeneracy point. There are also weak localization corrections to the conductivity, which are small for strong enough dephasing or for small enough systems. As shown in Ref. 26, it is convenient to decompose the retarded-advanced Cooperons in the singlet-triplet representation in both Σ and Λ channels. Then only singlets with respect to Σ matter. The general expression for the weak localization correction valid for arbitrary disorder then reads

$$\delta\sigma_{\mathrm{WL}} = -\frac{e^2}{\pi^2}\ln\left(\frac{L_{\mathrm{IR}}}{l}\right)[c_0 - 2c_\perp - c_z], \tag{53}$$

where l is the electron mean free path determined by the renormalized disorder and density of states, and L_{IR} is the infrared cutoff set by either the system size or the dephasing length. In Eq. (53), one has to put $c_i=1$ if disorder preserves the time-reversal (TR) invariance T_i and $c_i=0$ (meaning that the corresponding Cooperon modes are gapful) otherwise (see Table I). For a combination of several disorder types, only those Cooperon modes remain gapless that correspond to the TR symmetries preserved simultaneously by *all* disorder matrices involved. In particular, for the diagonal disorder α_0 all $c_i=1$ which yields antilocalization, whereas, e.g., for the combination of $\gamma_\perp$ and γ_z disorders we have $c_0=c_z=1$ and $c_\perp=0$, leading to the absence of the one-loop correction. On the other hand, for the combination of, e.g., β_z and γ_z disorders, $c_0=1$, $c_z=c_\perp=0$, and we get localization. Note that the weak localization correction is universal and depends only on the symmetry of the Hamiltonian.[68]

C. Unitary limit

In Sec. III B we have analyzed the behavior of the density of states and the conductivity in the case when impurities are weak, so that the disorder can be considered as Gaussian. [In terms of the action, Eq. (41), this amounted to keeping, after the ensemble averaging, only the $(\bar{\psi}\psi)^2$ term and neglecting all higher-order couplings.] In this subsection, we will consider the opposite case, when the electron is strongly scattered by an impurity and one has to deal with the complete T matrix (14). The analysis of the location of the "phase boundary" between the domains of weak and strong scatterers in the space of microscopic parameters of the problem is postponed to Sec. III D.

We proceed by first analyzing the results in the framework of the SCTMA, Sec. III A, and then discuss its accuracy and limitations. Like in the weak scatterer limit, the SCTMA can be simplified in the limit of strong scatterers. Specifically, at large U we neglect unity in comparison with $Ug(\varepsilon)$ in the denominator of Eq. (19) and obtain the self-consistency equation

$$\Sigma(\varepsilon) = \frac{\eta\Delta^2}{[\varepsilon - \Sigma(\varepsilon)]\ln\dfrac{-\Delta^2}{[\varepsilon-\Sigma(\varepsilon)]^2}}. \tag{54}$$

The parameter η is the dimensionless concentration of impurities defined as

$$\eta = \frac{\pi n_{\mathrm{imp}} v_0^2}{\Delta^2} \times \begin{cases} 1, & \text{short range}, \\ 4, & \text{long range}. \end{cases} \tag{55}$$

The scattering amplitude U does not enter Eq. (54). This means that the impurities are effectively considered infinitely strong, the limit that we will term the *self-consistent unitary approximation* (SCUA). For this type of impurities, the weak disorder assumption means that their concentration is small, $\eta \ll 1$.

The characteristic energy scale in the unitary limit is set by the value of Σ at zero energy: $\Sigma(\varepsilon=0) = \mp i\Gamma_\eta$, which we find to be

$$\Gamma_\eta \simeq \Delta\sqrt{\frac{\eta}{\ln(1/\eta)}}. \tag{56}$$

In contrast to its Born-limit counterpart Γ, which is exponentially small for $\alpha \ll 1$, the energy scale Γ_η depends on the disorder strength η in the power-law fashion. As we see below, this is intimately connected with a qualitatively different dependence of conductivity on the Fermi energy.

Further analysis of Eq. (54) can be performed in a way analogous to our treatment of the Born limit, Eq. (32). We get (see Ref. 61 concerning the crossover between high- and low-energy regimes)

$$\Sigma(\varepsilon) = \begin{cases} \mp i\Gamma_\eta + \dfrac{\eta\Delta^2 - 2\Gamma_\eta^2}{2(\eta\Delta^2 - \Gamma_\eta^2)}\varepsilon, & \varepsilon \ll \Gamma_\eta, \\ \dfrac{\eta\Delta^2}{2\varepsilon}\left[\dfrac{1}{\ln(\Delta/|\varepsilon|)} \mp \dfrac{i\pi\,\mathrm{sgn}\,\varepsilon}{2\ln^2(\Delta/|\varepsilon|)}\right], & \varepsilon \gg \Gamma_\eta. \end{cases} \tag{57}$$

Here upper (lower) signs correspond to the retarded (advanced) self-energy.

Using Eq. (57) and the relation between the Green function and the self-energy in the unitary limit, $g = -\eta\Delta^2/4\pi v_0^2\Sigma$, we get for the density of states, Eq. (20),

$$\rho_{\mathrm{SCUA}}(\varepsilon) = \frac{\eta\Delta^2}{\pi^2 v_0^2}|\mathrm{Im}\,\Sigma^{-1}(\varepsilon)| = \begin{cases} \dfrac{\eta\Delta^2}{\pi^2 v_0^2\Gamma_\eta}, & \varepsilon \ll \Gamma_\eta, \\ \dfrac{|\varepsilon|}{\pi v_0^2}, & \varepsilon \gg \Gamma_\eta. \end{cases} \tag{58}$$

The density of states is constant at small energy and shows a linear dependence characteristic for clean graphene at high energies. To find the disorder correction to this result, one has to use a more precise value of the self-energy than that given by Eq. (57). After two iterations of Eq. (54), the linear-in-η contribution to the density of states is obtained (see details in Appendix B),

$$\rho^{(1)}_{\mathrm{SCUA}}(\varepsilon) = \frac{|\varepsilon|}{\pi v_0^2}[1 - \alpha_U(\varepsilon)]. \tag{59}$$

Here the parameter α_U has the meaning of the inverse dimensionless conductance [see Eq. (63) below],

$$\alpha_U(\varepsilon) = \frac{\eta\Delta^2}{2\varepsilon^2 \ln^2(\Delta/|\varepsilon|)} \sim \frac{n_{\rm imp}\lambda_\varepsilon^2}{\ln^2(\Delta/|\varepsilon|)}. \tag{60}$$

It is of the order of the squared ratio of the electron wavelength λ_ε at energy ε to the distance between impurities, up to a logarithmic factor. The condition $\varepsilon \gg \Gamma_\eta$ ensures that the relative correction is small.

To find the correction to the density of states of the second order in η, one has to go beyond the self-consistent approximation. The diagrams with intersecting impurity lines become important in this case as we have already seen it in the Born limit (Sec. III B 2). A rigorous calculation taking into account all second-order diagrams is given in Appendix B. The result is

$$\rho^{(2)}(\varepsilon) = \frac{|\varepsilon|}{\pi v_0^2}\left[1 - \alpha_U(\varepsilon) - 2\alpha_U^2(\varepsilon)\ln\frac{\Delta}{|\varepsilon|}\ln\ln\frac{\Delta}{|\varepsilon|}\right]. \tag{61}$$

In order to calculate the conductivity, we find the polarization operator, Eq. (23),

$$\Pi^{RA}(\varepsilon) = \frac{1}{4\pi v_0^2}\frac{\eta\Delta^2}{2|\Sigma(\varepsilon)|^2}\frac{\varepsilon - 2\,\mathrm{Re}\,\Sigma(\varepsilon)}{\varepsilon - \mathrm{Re}\,\Sigma(\varepsilon)}. \tag{62}$$

Substituting it into Eq. (25), we obtain, for the conductivity at not too low energy, $\varepsilon \gg \Gamma_\eta$,

$$\sigma_{\rm SCUA}(\varepsilon) = \frac{4e^2\varepsilon^2}{\pi^2\eta\Delta^2}\ln^2\frac{\Delta}{|\varepsilon|}. \tag{63}$$

Equation (63) is written for the case of long-range disorder; if the disorder is short range, the vertex correction is absent and the resulting conductivity is twice smaller.

What about the multiple scattering of electrons on complexes of two or more impurities (described by mutually "entangled" T matrices, Appendix B) that are not included in the SCUA? We remind the reader that in the Born limit of weak impurities (Sec. III B 2), similar multiple-scattering processes contribute to the dominant (logarithmic) energy dependence of the conductivity, Eq. (49). In the unitary limit, however, the dominant energy dependence of the conductivity $\sigma(\varepsilon) \propto 1/\alpha_U(\epsilon)$ comes already from the ε dependence of a T matrix describing the scattering off a *single* impurity. Therefore, the logarithmic corrections to the conductivity, analogous to those in the Born limit [see Eq. (49)], are of minor importance in the unitary limit.

As in the case of Born-type disorder, Sec. III B, we now convert the energy dependence of conductivity into its dependence on the electron concentration n_e. We have according to Eq. (58) (for $\mu \gg \Gamma_\eta$)

$$n_e(\mu) = \frac{\mu|\mu|}{\pi v_0^2}, \tag{64}$$

so that Eq. (63) yields

$$\sigma(n_e) = \frac{e^2}{4\pi^2}\frac{|n_e|}{n_{\rm imp}}\ln^2\frac{\Delta^2}{v_0^2|n_e|}. \tag{65}$$

For the short-range disorder, the result is twice larger. In contrast to the limit of weak (Born) scatterers, the conductivity shows a strong concentration dependence: it varies linearly with n_e, with a logarithmic correction. This result compares nicely with the experimentally obtained linear behavior of $\sigma(n_e)$ (or, equivalently, constant mobility).[2,3] This indicates that the dominant scatterers are strong. Equation (65) predicts a logarithmic correction to the linear behavior, which should become more pronounced if the measurement is extended to larger gate voltages.

One can also calculate the SCUA conductivity at $\varepsilon \ll \Gamma_\eta$. In this limit, the contributions $\langle jG^R jG^R\rangle$ and $\langle jG^A jG^A\rangle$ should also be taken into account. The Drude conductivity then appears to have exactly the same value $\sigma_{\rm SCUA} = 2e^2/\pi^2\hbar$ as in the SCBA, Sec. III B 1. Analogously to the SCBA case, this result is questionable in view of the localization effects neglected in the Drude formalism. It is important to recall in this context that infinitely strong impurities are chiral (C_z), yielding a divergent density of states[70] (cf. Refs. 52 and 53) in this situation. We will return to the conductivity at half filling for a chiral disorder in Sec. IV.

D. Phase diagram

In the preceding subsections, Secs. III B and III C, we have studied the limits of weak (Born) and strong (unitary) scatterers, respectively. We have found that the behavior of the conductivity is essentially different in both limits: it depends only logarithmically on energy in the Born limit and shows a linear behavior (with a logarithmic correction) in the unitary limit. The aim of the present subsection is to construct a "phase diagram" that would predict which of these types of behavior is expected for given characteristics of disorder. (Of course, we do not mean any phases in the strict sense; there is a smooth crossover between the Born and unitary regimes.)

The unitary limit corresponds to the neglect of unity in comparison with $Ug(\varepsilon)$ in the denominator of Eq. (19). In order to see when this is justified, we use the large-energy expression (57) for $\Sigma(\varepsilon)$ and compare $Ug(\varepsilon)$ with 1. This yields the following energy-dependent value of the parameter η at the "phase boundary" between the weak scatterer and strong scatterer regimes,

$$\eta_c(\varepsilon) \sim \frac{\alpha\varepsilon^2}{\Delta^2}\ln^2\frac{\Delta}{|\varepsilon|}, \tag{66}$$

or, equivalently, $\alpha_U(\varepsilon) \sim \alpha$. For $\eta \ll \eta_c(\varepsilon)$—that is, $\alpha_U(\varepsilon) \ll \alpha$—the system is in the unitary limit.

In Fig. 6 we plot the phase diagram in both ε-η and ε-α coordinates. Remarkably, the system may pass from the Born into the unitary limit when the energy increases while the disorder remains fixed. In Fig. 6 (upper panel) this crossover occurs for a broad range of impurity concentrations, $\alpha^{-1}\exp(-1/\alpha) \ll \eta \ll \alpha$. At still smaller values of η the system is in the unitary phase at all energies. It is worth stressing that the unitary phase in Fig. 6 is established even for $\alpha \ll 1$, when disorder could be naively considered as weak. The reason for this effect is as follows. The growth of the density of states with increasing energy results in a more efficient scattering of higher-energy electrons by an impurity,

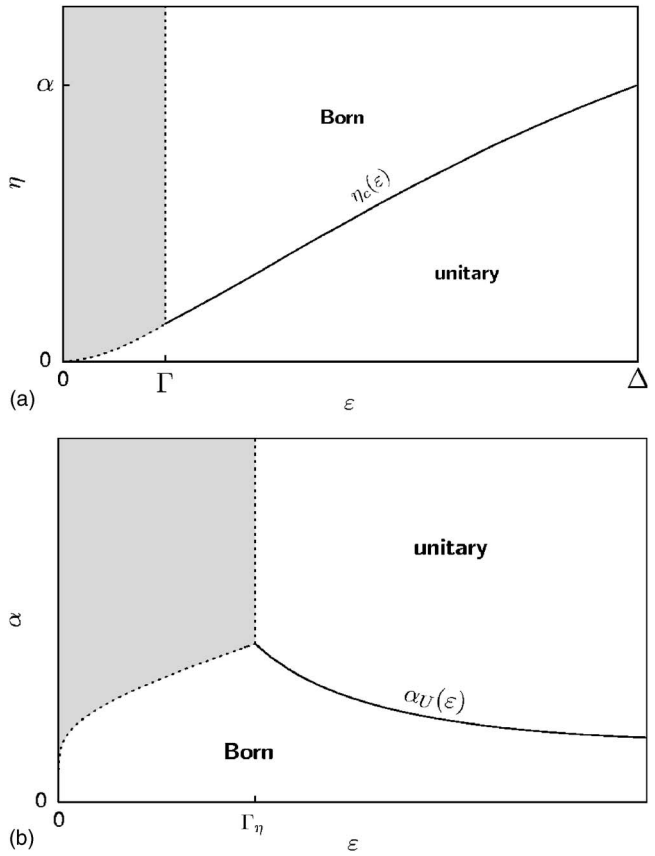

FIG. 6. "Phase diagram" in the ε-η plane for a fixed α (upper panel) and in the ε-α plane for a fixed η (lower panel). The solid line is the "phase boundary," Eq. (66) or (60), where the crossover between the Born and the unitary regimes takes place. At low energies (dashed part) the density of states saturates, while the Drude conductivity reaches a value $\sim e^2/h$, implying that generically the localization effects should become strong.

thus making the scatterer effectively stronger at higher energies. With increasing α the phase boundary (66) in Fig. 6 (upper panel) moves upwards, and for $\alpha \gtrsim 1$ the Born phase disappears altogether.

A unitary-to-Born crossover discussed above would manifest itself in a change of the behavior of the conductivity, from a linear energy dependence at high ε (Sec. III B) to a logarithmic dependence at lower energies (Sec. III C).[69] Experimentally, the measured conductivity of graphene shows a linear dependence down to the lowest-energy scale (where σ saturates at a value $\simeq e^2/h$). This indicates that the scattering is dominated by strong impurities, which remain in the unitary part of the phase diagram down to the lowest energies.

E. Charged impurities

The case of charged impurities deserves a special consideration. If such impurities are located far from the graphene layer, they are expected to be screened by the gate and will not be different from finite-range scatterers considered above. Let us consider, however, charged impurities located near the graphene layer. The scattering potential of the Coulomb center in 2D is $V_0(\mathbf{q})=2\pi e^2/\chi q$. Taking into account the static screening by the graphene electron gas in the random phase approximation (RPA), we obtain[71]

$$V(\mathbf{q}) = \frac{2\pi e^2}{\chi q + 2\pi e^2 \rho(\varepsilon)}, \tag{67}$$

where χ is the dielectric constant. Strictly speaking, the RPA is not justified in graphene since the parameter $r_s = e^2/\hbar v_0 \chi$ is of order unity. It will be sufficient, however, to find a parametric behavior of quantities of interest, up to numerical coefficients of order unity.

As follows from Eq. (67), the intervalley-scattering component of the Coulomb potential, $V(k_0) \simeq 2\pi e^2/\chi k_0$, is very small and can be neglected, so that the Coulomb impurities are of long-range type. As to the scattering within one valley, it is only slightly anisotropic. Indeed, the inverse screening length $\kappa = 2\pi e^2 \rho(\varepsilon)$ is of the same order as the characteristic momentum transfer, $\kappa \sim q \sim \varepsilon/v_0$ for $r_s \sim 1$. Therefore, up to a numerical factor of order unity, we can neglect q in the denominator of Eq. (67) (which means a neglect of the anisotropy of the intravalley scattering). This brings the screened charged impurities into the class of long-range scatterers considered above but with an energy-dependent amplitude,

$$U(\varepsilon) = \rho^{-1}(\varepsilon) \simeq \frac{\pi v_0^2}{|\varepsilon|}. \tag{68}$$

There is, however, an important difference between a charged impurity and a long-range potential impurity. The scattering amplitude for slow electrons, with momenta $q \lesssim |\varepsilon|/v_0$, is given by Eq. (68), while the electrons with larger momenta are scattered much less efficiently due to the lack of screening at small distances. This can be taken into account by setting an effective high-energy cutoff $\Delta \sim |\varepsilon|$.

Finally, using Eqs. (30), (55), and (66) with U from Eq. (68) and $\Delta \sim \varepsilon$, we obtain $\eta_c \sim \eta$. Thus we come to the conclusion that, with charged impurities, the system is just at the crossover between Born and unitary regimes. This also justifies the use of the clean density of states in Eq. (68). Indeed, approaching the crossover from the unitary side, the disorder-induced corrections to $\rho(\varepsilon)$ are negligible; see Eq. (59). On the other hand, if one uses the Born expression (48), logarithmic corrections are absent, as long as $\Delta \sim \varepsilon$, and the clean value of the density of states in Eq. (68) is again justified.

The energy and density dependences of the conductivity of graphene with Coulomb impurities are thus equivalently given by both Born [Eqs. (49) and (52) with energy-dependent coupling $\alpha_0 \sim n_{\mathrm{imp}} v_0^2/\varepsilon^2$] and unitary [Eqs. (63) and (65)] expressions with logarithms omitted,

$$\sigma \sim \frac{e^2\varepsilon^2}{n_{\mathrm{imp}} v_0^2} \sim \frac{e^2|n_e|}{n_{\mathrm{imp}}}. \tag{69}$$

The Born approximation was used for calculating the conductivity in recent works, Refs. 16 and 30 (see also Ref. 34). The result is consistent with Eq. (69). A different result (containing an additional logarithmic factor) was obtained in Ref. 72. We believe that the derivation in Ref. 72 is incorrect[73] since it employs the quasiclassical Thomas-Fermi approxi-

mation beyond its range of validity (at energies much larger than ϵ_F).

IV. CONDUCTIVITY AT THE DEGENERACY POINT: CHIRAL DISORDER

A. Universal conductivity

1. Preliminaries

In this section we consider the conductivity of graphene at half filling, $\varepsilon=0$. The Drude conductivity obtained self-consistently in Sec. III in both Born and unitary limits has the value $\sigma=2e^2/\pi^2\hbar$ at this point. Since this value is of the order of conductance quantum, this is by no means the end of the story: the localization effects become strong at half filling. If the intervalley scattering is weak (long-range disorder potential), an intermediate temperature range exists where the conductivity correction is positive[21,26,32,74] due to the additional Berry phase π associated with the electron pseudospin in the sublattice space. This situation belongs to the symplectic symmetry class. With lowering temperature T, the intervalley scattering comes into play and a crossover to the orthogonal symmetry class occurs.[26,32,33] The localization correction becomes negative and drives the system into the strong localization regime.[32] Thus, for a generic disorder, the conductivity at half filling should have a pronounced temperature dependence and get strongly suppressed with lowering T. Surprisingly, this is not what is observed in the experiment. The conductivity has been found[2,3] to be close to the value $4e^2/h$, remaining T independent in a broad range of temperatures. The aim of this section is to analyze whether and in what situation this behavior may be expected theoretically. According to what was said above, this might only happen, if at all, for a particular type of disorder.

The special class of disorder that we will consider in this section is the randomness that preserves one of the chiral symmetries (13) of the clean graphene Hamiltonian. Some possible realizations of such type of disorder were listed in Sec. II C. Whether the dominant disorder in graphene may be of this kind is an open issue, which may be related to technological aspects of the sample preparation. Our aim here will be to analyze what are consequences of the assumption of chiral character of disorder.

A peculiar behavior of 2D systems with chiral disorder with respect to localization effects has been demonstrated by Gade and Wegner.[75,70] They considered a random hopping problem on a square lattice and showed that at zero energy, where the system possesses chiral symmetry, the RG β function of the corresponding σ model vanishes to all orders in the inverse conductivity, implying that the conductivity is not renormalized. This absence of the usual infrared-singular corrections to the conductivity due to Cooperon and diffuson loops can be attributed to the fact that the "antilocalizing" interference corrections to the density of states cancel the localization corrections to the diffusion coefficient. The density of states has been found[45,70,77,78] to diverge as $\rho(\varepsilon) \sim \varepsilon^{-1}f(\varepsilon)$ for $\varepsilon\to 0$, where $f(\varepsilon)$ gives the subleading ε dependence and provides the convergence of the total number of electronic states.[76] At any finite ε the chiral symmetry is broken and localization on the scale $\xi(\varepsilon)\propto|f(\varepsilon)|^{-1/2}$ occurs.[70] The states at the band center $\varepsilon=0$ are delocalized and the conductivity $\sigma(\varepsilon=0)$ takes a finite value depending on the disorder strength. According to the classification of Refs. 66, 79, and 80, the system studied in Refs. 70 and 75 belongs to the chiral symmetry class AIII.

While the results of Refs. 70 and 75 suggest that one may expect a finite zero-energy conductivity in our problem, they cannot be directly applied. Indeed, the dimensionless Drude conductivity at $\varepsilon=0$ is of order unity in our case, whereas it should be large to justify the derivation of the σ model and of the corresponding (diffusive) perturbative RG. Another related peculiarity of the problem we are considering is the Dirac dispersion of carriers. This will allow us to prove below a statement that is still stronger than that of Gade and Wegner: we will show that for certain types of chiral disorder all disorder-induced contributions to conductivity cancel.

2. C_0 chirality: Symmetry consideration

Let us consider the disorder which preserves the C_0 chirality, $H=-\sigma_3 H\sigma_3$. The random part of the Hamiltonian contains the matrices $\sigma_{1,2}\tau_3$, $\sigma_{1,2}\tau_{1,2}$, and $\sigma_{1,2}\tau_0$. According to Table I, in the case of weak disorder, the corresponding coupling constants are $\alpha_\perp$, $\beta_\perp$, and $\gamma_\perp$. While the disorder characterized by $\beta_\perp$ and $\gamma_\perp$ preserves the time-reversal invariance T_0, the $\alpha_\perp$ disorder, being physically a random vector potential, violates the T_0 symmetry.

According to Ref. 81, the random Dirac Hamiltonians preserving the C_0 chirality and violating the TR symmetry (case 1 of Ref. 81) belong to the chiral symmetry class AIII, while the combination of C_0 chirality and T_0 symmetry (case 6 of Ref. 81) drives the system into the Bogolyubov–de Gennes symmetry class CI. In both cases, the low-energy theory (σ model) is affected by the presence of the Wess-Zumino-Novikov-Witten term in the action.

The one-loop RG equations for C_0 disorder read (see Appendix A)

$$\frac{\partial\alpha_\perp}{\partial\ln L}=0, \tag{70}$$

$$\frac{\partial\beta_\perp}{\partial\ln L}=4\beta_\perp\gamma_\perp, \tag{71}$$

$$\frac{\partial\gamma_\perp}{\partial\ln L}=\beta_\perp^2. \tag{72}$$

Note that Eq. (70) for $\alpha_\perp$ is split from Eqs. (71) and (72). This set of equations is identical to Eq. (19) of Ref. 66 with $g'=\alpha_\perp$, $g=2\gamma_\perp$, $g_{\pi 0}=0$, and $g_{\pi\pi}=2\beta_\perp$. In Ref. 66, these couplings described the scattering between the four nodal points of the spectrum of a disordered d-wave superconductor. Our problem with only two nodes corresponds to setting the coupling between the neighboring nodes in d-wave superconductors to zero, $g_{\pi 0}=0$, while retaining the forward-scattering (intranode, g) and backscattering (scattering between the opposite nodes, $g_{\pi\pi}$) amplitudes. This situation (non-Abelian vector potential problem) was considered

in Ref. 64 (see also Refs. 82–84), where the density of states was shown to vanish in the limit $\varepsilon \to 0$ as

$$\rho(\varepsilon) \propto |\varepsilon|^{1/7}. \tag{73}$$

Here $1/7=1/(2N^2-1)$, where $N=2$ is the number of flavors (nodes).

In the presence of the random vector potential only ($\alpha_\perp$ coupling, preserving all four chiralities simultaneously, class AIII), the density of states also goes to zero with decreasing energy, but with a nonuniversal exponent[63,64] which depends on $\alpha_\perp$:

$$\rho(\varepsilon) \propto |\varepsilon|^{(1-\alpha_\perp)/(1+\alpha_\perp)}. \tag{74}$$

Note that in this random vector potential problem, the disorder strength remains nonrenormalized; see Eq. (70) (in fact, the one-loop equations for $\alpha_\perp$ and ε are exact; see Refs. 45 and 63). Therefore, $\alpha_\perp$ does not generate the scale Γ and the one-loop result for the density of states, Eq. (74), holds in the whole range of energies below Δ.

3. C_0 chirality: Conductivity at the Dirac point

We are now going to study the conductivity in the situation when disorder preserves C_0 chirality. The chiral symmetry C_0 allows one to relate retarded and advanced Green functions:

$$\sigma_3 G^{R(A)}(\varepsilon;\mathbf{r},\mathbf{r}')\sigma_3 = -G^{A(R)}(-\varepsilon;\mathbf{r},\mathbf{r}'). \tag{75}$$

The conductivity is given by the Kubo formula (21), which we rewrite here in the full form

$$\sigma^{xx} = \frac{1}{\pi}\int d^2(r-r')\mathrm{Tr}\Big[j^x G^R(0,\mathbf{r},\mathbf{r}') j^x G^A(0,\mathbf{r}',\mathbf{r}) - \frac{1}{2} j^x G^R(0,\mathbf{r},\mathbf{r}') j^x G^R(0,\mathbf{r}',\mathbf{r}) - \frac{1}{2} j^x G^A(0,\mathbf{r},\mathbf{r}') j^x G^A(0,\mathbf{r}',\mathbf{r})\Big]. \tag{76}$$

Now we use the identity (75) to trade all advanced Green functions in Eq. (76) for retarded ones and thus to present the conductivity in terms of retarded Green functions only. Further, we exploit the following important relation between the components of the current operator (22):

$$\sigma_3 j^x = -j^x \sigma_3 = i j^y, \tag{77}$$

which is a consequence of the Dirac spectrum. At this point, our problem differs from that considered by Gade and Wegner[70,75] who dealt with a bipartite *square* lattice with a nonlinear electronic spectrum.

The transformations (75) and (77) allow us to cast the Kubo formula in the following form:

$$\sigma^{xx} = -\frac{1}{\pi}\sum_{\alpha=x,y}\int d^2(r-r') \times \mathrm{Tr}[j^\alpha G^R(0;\mathbf{r},\mathbf{r}') j^\alpha G^R(0;\mathbf{r}',\mathbf{r})]. \tag{78}$$

At first glance, this expression is zero due to the gauge invariance. Indeed, the right-hand side of Eq. (78) is proportional to the second derivative of the partition function $Z[\mathbf{A}]=\mathrm{Tr}\ln G^R[\mathbf{A}]$ (or, equivalently, first derivative of the current $\mathrm{Tr} j^\alpha G^R[\mathbf{A}]$) with respect to the constant vector potential $\mathbf{A}$. The gauge invariance implies that a constant vector potential does not affect gauge-invariant quantities like the partition function or the current, so that the derivative is zero. This argument is, however, not fully correct, in view of a quantum anomaly present in this problem. The elimination of $\mathbf{A}$ amounts technically to a shift in the momentum space $\mathbf{k}\to\mathbf{k}-e\mathbf{A}$, which naively does not change the momentum integral. If we consider a formal expansion in the disorder strength, this argument will indeed hold for all terms involving disorder but not for the zeroth-order contribution. The momentum integral $\int d^2k \mathrm{Tr} j^\alpha G_0^R(\mathbf{k})$ is ultraviolet divergent and the shift of variable is illegitimate. This anomaly was first identified by Schwinger[85] for (1+1)-dimensional massless Dirac fermions. In the Schwinger model, the polarization operator is not affected by an arbitrary external vector potential $\mathbf{A}(x,t)$ and is given by the anomalous contribution, yielding a photon mass in the 1+1 electrodynamics.[85,86] In our analysis, the role of $\mathbf{A}(x,t)$ is played by the chiral disorder. The explicit calculation of the zeroth-order diagram (the one with no disorder included) yields

$$\sigma = -\frac{8e^2v_0^2}{\pi}\int \frac{d^2k}{(2\pi)^2}\frac{\delta^2}{(v_0^2k^2+\delta^2)^2} = \frac{2e^2}{\pi^2} \equiv \frac{4e^2}{\pi h}. \tag{79}$$

(In the last expression we have restored the Planck constant to follow the convention of expressing the conductivity in units of the conductance quantum e^2/h.) Here δ is an infinitesimal imaginary part in the denominator of the Green function; we will return to its role and physical meaning below. Let us emphasize that our proof of Eq. (79) relies only on the C_0 symmetry of the disorder and does not assume its Gaussian character. We note that the same universal value of the conductivity in the situation when the only type of disorder is the Abelian random vector potential ($\alpha_\perp$) was previously obtained in Ref. 63. For a non-Abelian gauge potential with Gaussian statistics and equal couplings, $\alpha_\perp=\gamma_\perp=\beta_\perp/2$, universal conductivity was obtained in Ref. 82 by using the mapping onto a Wess-Zumino-Novikov-Witten model.

An alternative derivation of the same result is based on the Ward identity

$$-ie(\mathbf{r}-\mathbf{r}')G^R(0;\mathbf{r},\mathbf{r}') = [G^R\mathbf{j}G^R](0;\mathbf{r},\mathbf{r}'). \tag{80}$$

Averaging it over disorder, plugging it into Eq. (78), transforming to the momentum space, and performing the integration by parts, we are left with the surface contribution only,

$$\sigma = -\frac{ev_0}{4\pi^3}\oint d\mathbf{k}_n \mathrm{Tr}[\mathbf{j}G^R(\mathbf{k})], \tag{81}$$

where the integral is taken over a large circle $|\mathbf{k}|=\mathrm{const}\to\infty$. For large momenta the Green function can be replaced by its bare value, which yields again the universal conductivity

$$\sigma = \frac{e^2}{\pi^3} \oint \frac{d\mathbf{k}_n \mathbf{k}}{k^2} = \frac{2e^2}{\pi^2} \equiv \frac{4e^2}{\pi h}. \tag{82}$$

This universal value of the conductivity is independent of the ultraviolet cutoff in the momentum space. This signifies that the integral in Eq. (78) is accumulated in the vicinity of the degeneracy point, as seen explicitly in Eq. (79). The fact that, in a realistic system, the linearization of the spectrum ceases to be valid at high momenta does not spoil the derivation: the functions G^R and G^A are essentially equal to each other there, so that the integrand of Eq. (76) is canceled.

It is worth emphasizing that the derivation of Eq. (82) assumes that the ultraviolet cutoff Δ is much larger than the disorder-induced energy scale Γ. (More accurately, here Γ is the low-energy electron relaxation rate determined as a scale where the dimensionless Drude conductivity is of order unity or, equivalently, where the RG flow enters the strong coupling regime.) In other words, the disorder is weak—i.e., $\alpha \ll 1$ for Gaussian disorder. One more formulation of this condition is that for energies comparable to the cutoff, $\varepsilon \sim \Delta$, the Drude conductivity considered in Sec. III is large (compared to e^2/h). This condition, which we assume throughout the paper, is very well fulfilled in the experiments.[2,3] Violation of this condition would imply that the disorder is so strong that it completely destroys the Dirac character of the spectrum. In this situation the universal value of the conductivity (79) and (82) of the chiral-symmetric system would not survive. The corrections to the universal value of the conductivity are exponentially small, $\delta\sigma \lesssim e^2\Gamma/\Delta$, which implies that there are no corrections to any order in the perturbative expansion of $\sigma(\varepsilon=0)$ in $\alpha \ll 1$.

The above derivation of the universal conductivity remains valid for the case when a magnetic field of an arbitrary strength is applied: the vector potential A_α couples to the current—i.e., to the matrices $\tau_3\sigma_\alpha$, $\alpha=x,y$—thus preserving the chiral symmetry. In this context, it is worth mentioning the result of Hikami, Shirai, and Wegner[87] who found that the longitudinal conductance in the center of the lowest Landau level of chiral-disordered 2D electron gas is equal exactly to $\sigma=2e^2/\pi^2\hbar$ in the limit of a very strong magnetic field, when the Landau level mixing can be neglected. Their finding can be considered as a $B\to\infty$ limit of our general result. Indeed, in this limit the kinetic energy is frozen, so that the difference between the electron dispersion on the square lattice (considered in Ref. 87) and the graphene lattice becomes immaterial.

We turn now to an important and delicate point related to the above derivation of the universal conductivity (79). Specifically, we have introduced an infinitesimally small imaginary part of the energy, δ. Physically, it has the meaning of the electron lifetime or, alternatively, a dephasing rate, and can be thought as modeling processes of escape of electrons in some reservoir or some dephasing mechanism. Models with such a uniform constant value of δ were used in the literature to imitate dephasing in quantum dots; see, e.g., Ref. 88.

In our calculation, δ has served as an infrared regulator for the theory. Although it has dropped from the final result, its role is not completely innocent. Depending on the physical situation, the infrared regularization may be provided by different quantities, which, as we are going to discuss, will influence the value of the conductivity. Specifically, in addition to δ, we can imagine the following sources of the infrared cutoff: (i) finite frequency, (ii) finite system size, and (iii) interaction-induced dephasing at finite temperature. In Sec. IV B we will analyze the frequency dependence of the conductivity. As to the situations when the temperature or the system size governs the infrared behavior, we restrict ourselves to brief comments only, relegating a detailed analysis to future work.

4. C_z chirality

Let us now turn to the disorder which preserves the C_z chirality, $H=-\sigma_3\tau_3 H \sigma_3\tau_3$. The random part of the Hamiltonian may then contain matrices $\sigma_3\tau_{1,2}$, $\sigma_{1,2}\tau_3$, $\sigma_{1,2}\tau_0$, and $\sigma_0\tau_{1,2}$. The first two (the corresponding coupling constants are β_0 and $\alpha_\perp$) violate the time-reversal symmetry T_0; the last two ($\gamma_\perp$ and β_z) preserve it (see Table I). Note that the disorder characterized by $\alpha_\perp$ and $\gamma_\perp$ (real and imaginary vector potentials, respectively) also preserves the chiral symmetry C_0 considered above.

According to Ref. 81, random Dirac Hamiltonians preserving the C_z chirality and violating the TR symmetry (case 2 of Ref. 81) belong to the chiral unitary symmetry class AIII. The combination of C_z chirality and the time-reversal invariance T_0 (case 9_+ of Ref. 81) corresponds the chiral orthogonal symmetry class BDI. Finally, the combination of C_z chirality and T_z symmetry (case 9_- of Ref. 81) falls into the chiral symplectic symmetry class CII.

The one-loop RG equations for C_z disorder read (see Appendix A)

$$\frac{\partial \alpha_\perp}{\partial \ln L} = 2\beta_0\beta_z, \tag{83}$$

$$\frac{\partial \beta_0}{\partial \ln L} = 2\alpha_\perp(\beta_0+\beta_z), \tag{84}$$

$$\frac{\partial \beta_z}{\partial \ln L} = 2\alpha_\perp(\beta_0+\beta_z), \tag{85}$$

$$\frac{\partial \gamma_\perp}{\partial \ln L} = \beta_0^2+\beta_z^2. \tag{86}$$

This model was considered in Ref. 45; the RG equations (83)–(86) agree with the set of equations (4.84) in Ref. 45 with $g_\mu=\beta_0/\sqrt{2}$, $g_{A'}=\alpha_\perp$, $g_A=\gamma_\perp$, and $g_m=\beta_z/\sqrt{2}$. If the system is time-reversal (T_0) invariant, only the couplings β_z and γ_z survive; this case was considered in Refs. 45 and 89. The density of states in the generic C_z case diverges[45,70,75–78] in the limit $\varepsilon\to 0$; see Sec. IV A 1 [for the case of the random vector potential, see Eq. (74)].

Let us turn to the conductivity at half filling for a generic disorder preserving the C_z chirality. The proof of the universality of the conductivity based on gauge-invariance arguments does not work now. Indeed, the C_z-chirality transformation of the Green's function,

$$\sigma_3\tau_3 G^{R(A)}(\varepsilon;\mathbf{r},\mathbf{r}')\sigma_3\tau_3 = -G^{A(R)}(-\varepsilon;\mathbf{r},\mathbf{r}'), \tag{87}$$

generates the new vector vertices $j^{x,y}\tau_3$ instead of currents (these new vertices can be considered as $\mathbf{j}_5$ currents of Dirac fermions). Then we are left with the G^RG^R-type correlators of both $j^{x,y}$ and $j_5^{x,y}$. The latter cannot be obtained as derivatives of the partition function with respect to the constant vector potential $\mathbf{A}$. Nevertheless, for weak disorder we find that the conductivity at half filling is still universal,

$$\sigma = \frac{4e^2}{\pi h}, \tag{88}$$

up to corrections in powers of disorder strength. Recently, this result was also obtained in Ref. 90.

To show this, we first calculate the perturbative correction $\delta\sigma^{(1)}$ to the conductivity of a pure system at the first order in disorder strength and find that it vanishes, $\delta\sigma^{(1)}=0$. This implies that the conductivity at $\varepsilon=0$ does not depend on the ultraviolet cutoff Δ. Indeed, all the contributions generated by the RG (and thus depending on the ratio Δ/δ) sum up to zero, because we can use the fully renormalized disorder as an effective single-impurity line in $\delta\sigma^{(1)}=0$. The second-order perturbative calculation yields

$$\delta\sigma^{(2)} = \frac{e^2}{\pi h}(\beta_0 - \beta_z)^2. \tag{89}$$

We note that the combination $\beta_0-\beta_z$ is not renormalized during the RG procedure, as follows from Eqs. (84) and (85). This is in agreement with the above RG argument for the first-order correction. Thus the conductivity at the Dirac point can be presented as a series in the parameter $\beta_0-\beta_z$. Next, we recall that for C_z chirality, the RG β function of the Gade-Wegner σ model[70,75] vanishes to all orders, so that there are no singular quantum-interference corrections to $\sigma(\varepsilon=0)$ due to the soft modes (impurity ladders). This proves that the expansion of $\sigma(\varepsilon=0)$ in powers of $\beta_0-\beta_z$ converges. Thus for the case of weak disorder the conductivity is universal with small corrections in powers of the disorder strength (unlike in the case of the C_0 chirality, where the corrections are nonperturbative in the disorder strength).

5. $C_\perp$ chirality and decoupled valleys

Finally, let us discuss the case of $C_{x,y}$ chirality (couplings $\alpha_\perp$, γ_0, and γ_z). Each of these chiralities taken separately is similar to the C_z chirality. However, in an isotropic system considered here, both C_x and C_y chiralities are expected to be present simultaneously. This implies that the disordered Hamiltonian anticommutes with both τ_1 and τ_2 and hence is proportional to τ_3. Thus it is split into two equivalent copies. Therefore, the symmetry of the problem is governed by the properties of the "sub-Hamiltonians" and its chirality is in fact fictitious. In particular, the generic case with all $\alpha_\perp$, γ_0, and γ_z present[63] corresponds to the conventional Gaussian unitary class A (quantum Hall effect). A single coupling γ_z corresponds to the symmetry class D (random mass problem). In all these cases the system is in a critical phase so one can expect a finite conductivity at $\varepsilon=0$. For the sake of completeness we present the RG equations for the $C_\perp$ chirality:

$$\frac{\partial\alpha_\perp}{\partial\ln L} = 4\gamma_0\gamma_z, \tag{90}$$

$$\frac{\partial\gamma_0}{\partial\ln L} = 2(\alpha_\perp+\gamma_0)(\gamma_0+\gamma_z), \tag{91}$$

$$\frac{\partial\gamma_z}{\partial\ln L} = 2(\alpha_\perp-\gamma_z)(\gamma_0+\gamma_z). \tag{92}$$

We are not aware of realistic examples of the disorder preserving the $C_\perp$ chirality in the context of the transport in disordered graphene. Therefore, we will not consider this case in the rest of the paper.

We would like to stress, however, that the $C_\perp$ chirality is in fact a particular case of a more general class of disorder (couplings α_0, $\alpha_\perp$, α_z, γ_0, $\gamma_\perp$, γ_z) that does not mix the two valleys K and K'. The conductivity is then determined by the symmetric combinations $\alpha_\mu+\gamma_\mu$ only, and the RG equations have the same form (90)–(92) with a replacement $\alpha_\perp\to\alpha_\perp+\gamma_\perp$, $\gamma_0\to\alpha_0+\gamma_0$, $\gamma_z\to\alpha_z+\gamma_z$. This implies that, if at least two of $\alpha_\mu+\gamma_\mu$ couplings are present, the electrons in each valley are at the quantum Hall critical point[63] characterized by a finite longitudinal conductivity $\sim e^2/h$. Note that the Hall conductivity is absent due to the cancellation between the two independent valleys. Thus, a universal conductivity $\sim e^2/h$ can emerge not only for a chiral disorder but also when the randomness does not mix the two valleys. We relegate a more detailed study of the latter case to a separate publication and return to C_0 and C_z chiralities below.

B. Conductivity at finite frequency

In this subsection, we analyze the frequency dependence of the conductivity. For completeness, we also keep a small level width δ introduced above. It was crucial for the argument leading to Eq. (79) that the system be exactly at half filling, $\varepsilon=0$. A nonzero frequency implies an integration over the energy range of the width ω, which breaks the chiral symmetry. When the frequency ω is much smaller than δ, this effect is, however, negligible, the infrared regularization is provided by δ, and the universal result (79) survives. In its turn, δ plays no role when $\omega\gg\delta$: it is the frequency that serves as a dominant infrared cutoff now. In the high-frequency limit $\omega\gg\Gamma$, the situation simplifies again: one can neglect the effect of disorder altogether and calculate the conductivity by a simple Kubo formula with bare Green functions. The result for the real part of the conductivity is again universal but with a slightly larger value:[31,63]

$$\begin{aligned}\mathrm{Re}\,\sigma(\omega\gg\Gamma) &= \frac{2}{\pi}\int_0^\omega \frac{d\varepsilon}{\omega}\int\frac{d^2k}{(2\pi)^2} \\ &\quad\times \mathrm{Tr}[j^x \mathrm{Im}G_0^R(\varepsilon-\omega,\mathbf{k})j^x \mathrm{Im}G_0^R(\varepsilon,\mathbf{k})] \\ &= 8\pi e^2 v_0^2\int_0^\omega\frac{d\varepsilon}{\omega}\int\frac{d^2k}{(2\pi)^2}|\varepsilon-\omega|\delta[(\varepsilon-\omega)^2 \\ &\quad - k^2]|\varepsilon|\delta[\varepsilon^2-k^2] = \frac{e^2}{4} \equiv \frac{\pi e^2}{2h}.\end{aligned} \tag{93}$$

A very interesting new situation arises in the intermediate regime $\delta \ll \omega \ll \Gamma$. Here ω plays a twofold role, leading to two competing effects. On the one hand, as discussed above, the frequency drives the system away from the chiral-symmetric point and thus restores localization. On the other hand, the frequency cuts off the singular localization correction. Which of these effects wins? To answer this question, one should compare ω with the level spacing in the localization area, $\Delta_\xi(\varepsilon)$, where $\varepsilon \sim \omega$. In order to find the scaling of Δ_ξ with energy, we consider a RG transformation that drives the system away from the chiral fixed point. The RG stops when the renormalized energy $\tilde{\varepsilon}$ reaches the macroscopic scale Δ; on such scales, the disorder becomes already strong since the initial value of ε was below Γ. In this strongly disordered case, the value of the running ultraviolet cutoff length Lv_0/Δ (corresponding to the renormalized electron wavelength) determines then the localization length ξ. As discussed in Sec. III B 2, the density of states ρ scales as $\varepsilon^{-1}L^2$. Therefore,

$$\frac{\rho\varepsilon}{(v_0/\Delta)^2} \sim \frac{\tilde{\rho}\tilde{\varepsilon}}{\xi^2}, \tag{94}$$

implying for the level spacing at the length ξ,

$$\Delta_\xi(\varepsilon) \equiv \frac{1}{\rho(\varepsilon)\xi^2(\varepsilon)} \sim \varepsilon \sim \omega. \tag{95}$$

This result is rather general and is only based on the fact that the operator governing the flow of the system away from criticality couples to the energy in the action. One can of course explicitly verify that the results of Ref. 70 for the density of states and the localization length quoted in Sec. IV A 1 satisfy Eq. (95).

We conclude that the two competing effects of the frequency (the localization and the infrared regularization) "make a draw"—both of them are equally important. Therefore, the system turns out to be, roughly speaking, halfway between the chiral fixed point and the conventional symmetry. This results in a new universal (frequency-independent) value of the conductivity $\sigma_\omega \sim e^2/h$ in the considered regime $\delta \ll \omega \ll \Gamma$. More precisely, this value depends on the type of chirality and the symmetry class of the system away from the degeneracy point. In particular, the system with generic C_0- and C_z-chiral disorder with (without) TR symmetry T_0 is driven into the Wigner-Dyson orthogonal (respectively, unitary) symmetry class by finite energy. On the other hand, the system with C_z- and T_z-invariant disorder (β_0 and $\gamma_\perp$) falls into the Gaussian symplectic symmetry class away from $\varepsilon = 0$.

The frequency dependence of the conductivity at the Dirac point is sketched in Fig. 7. Remarkably, $\mathrm{Re}\sigma(\omega)$ is of the order of e^2/h in the whole range of frequencies, taking three different values: $\sigma = 4e^2/\pi h$ at low frequencies ($\omega \ll \delta$), $\mathrm{Re}\,\sigma = \pi e^2/2h$ at high frequencies ($\omega \gg \Gamma$), and $\mathrm{Re}\,\sigma = \sigma_\omega$ in the intermediate range. Despite its universality (for a given symmetry), the value σ_ω most likely cannot be calculated analytically, since this would require an exact knowledge of the full crossover between the chiral and the normal classes.

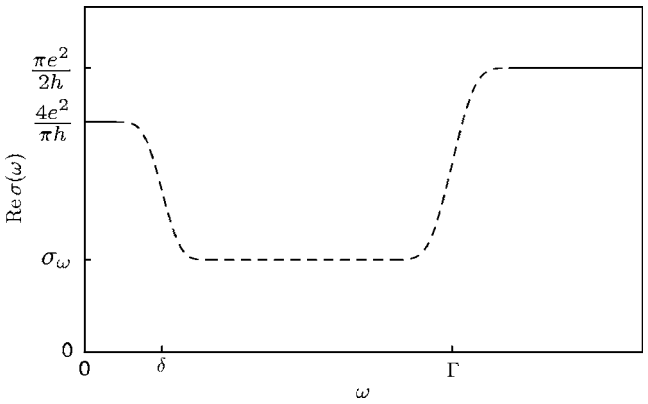

FIG. 7. Frequency dependence of conductivity in a system with chiral disorder at half filling. At intermediate frequency $\delta \ll \omega \ll \Gamma$, the conductivity acquires some universal value σ_ω of the order of e^2/h which is not known analytically. This value depends on the type of chirality and the symmetry class of the system away from the degeneracy point.

C. Additional comments

In Secs. IV A and IV B we have analyzed the conductivity in the case when the dominant infrared regularization is provided either by the inverse life time δ or by the frequency ω. As has been mentioned above, this role may be alternatively played by the interaction-induced dephasing at finite temperature or by the finite size of the system. Leaving a detailed analysis of these problems for the future, we only make some comments on them in Secs. IV C 1 and IV C 2 below. Finally, in Sec. IV C 3 we briefly discuss what happens with the problem considered when we pass from the 2D geometry to the quasi-1D one by rolling the plane into a cylinder.

1. Temperature dependence

In the presence of interactions, the temperature T plays a twofold role, similarly to the frequency. On the one hand, it induces an averaging over the energy window of width $\sim T$, thus breaking the chiral symmetry and "switching on" the localization effects. On the other hand, the interaction at finite T generates a nonzero dephasing rate $\tau_\phi^{-1}(T)$ cutting off the localization corrections. As we showed in Sec. IV B, the level spacing $\Delta_\xi(T)$ is $\sim T$, so that the result of the competition of these two effects depends on the value of $T\tau_\phi(T)$. The theory of dephasing in the present situation remains to be developed. If the dominant mechanism of dephasing is the electron-electron interaction, one can expect that (like in conventional 2D systems with dimensionless conductivity replaced by unity) $\tau_\phi^{-1}(T) \sim T$. If this is indeed true, the behavior of the conductivity at $T < \Gamma$ will be qualitatively analogous to that for the case of finite frequency, Sec. IV B. In particular, in the experimentally relevant range $\delta \ll T \ll \Gamma$ the conductivity will take a temperature-independent value $\sigma_T \sim e^2/h$. At high temperatures $T > \Gamma$, the T dependence of the conductivity will essentially reproduce its ε dependence for given type of disorder (Born or unitary).

More realistically, one can think about a situation when the disorder is predominantly chiral, but the chiral symmetry

is slightly broken,[51,53] e.g., by weak potential disorder on the energy scale $\Gamma_\chi \ll \Gamma$. Then the above consideration allowing one to expect the conductivity $\sigma_T \sim e^2/h$ will be applicable in the intermediate range $\Gamma_\chi < T < \Gamma$; at still lower temperatures $T \ll \Gamma_\chi$, the chirality-breaking effects will drive the system into the strong localization regime.

It is worth noting that the interaction may lead to other effects (in particular, to open the gap in the spectrum and/or to break the chiral symmetry; cf. Refs. 25 and 91) not included in our consideration. These questions also require further study.

2. Mesoscopic sample

Let us now consider the situation when all the potential infrared regulators δ, T, and ω are much smaller than the level spacing in the sample. In this case, the sample will be fully phase coherent (mesoscopic) and its size will serve as an infrared cutoff. In such a mesoscopic situation one should in general speak about a conductance, not conductivity. Furthermore, the properties of the conductance will essentially depend on the sample geometry. Consider a rectangular sample $L_x \times L_y$, with current flowing along the x axis. For an approximately square sample $L_x \sim L_y$ we expect, based on the above results, an average conductance of order e^2/h. Indeed, one can imagine taking first δ larger than the level spacing (so that the result of Sec. IV A applies) and then decreasing it until it reaches the level spacing. The above statement follows from the continuity. In view of the mesoscopic character of the sample, we also expect in this case a broad distribution of the conductance, with a variance of the order of $(e^2/h)^2$. Both the average value and the conductance distribution will depend on the exact value of the aspect ratio L_x/L_y in a nontrivial way and can hardly be calculated.

For a long sample $L_x \gg L_y$, the geometry becomes quasi-one-dimensional and our results for the universal conductivity $\sim e^2/h$ cease to be relevant (see also Sec. IV C 3).

Finally, let us consider a case of a very broad and short sample $L_y \gg L_x$. In this situation, the conductance will be self-averaging, so that one can again speak about conductivity. Using again the continuity, we conclude that the conductivity in this situation will have some universal value $\sigma_L \sim e^2/h$. Whether this value is equal to the above universal conductivity $4e^2/\pi h$, Eq. (79), or the numerical coefficient is different, requires further study. Remarkably, the same value, Eq. (79), has been found[11,22,90] for the conductance of a *clean* graphene sample in the considered geometry $L_y \gg L_x$.

3. Cylindric geometry

Let us take a C_0-symmetric strip of a large transverse size L_y and infinite in the x direction, and roll if into a cylinder, preserving the chiral structure. Let us further assume a small but nonzero level width δ, as in Sec. IV A. If δ is much larger than the level spacing in the square $L_y \times L_y$, the system is effectively two dimensional and the consideration of Sec. IV A applies. Let us consider the opposite limit. One can then ask whether our result concerning the universal conductivity will be applicable in this quasi-1D geometry. Analyzing the derivation in Sec. IV A it is not difficult to see that it breaks down: the momentum q_y is now quantized and its shift therefore not allowed. Let us consider, however, an Aharonov-Bohm flux Φ piercing the cylinder, which amounts to introducing the extra phase $e^{i\Phi/\Phi_0}$ in the periodic boundary conditions (Φ_0 is the flux quantum). Averaging over Φ, we restore the applicability of the consideration of Sec. IV A, so that

$$\langle \sigma \rangle_\Phi = \frac{4e^2}{\pi h}. \tag{96}$$

Therefore, depending on the value of the Aharonov-Bohm flux, the conductivity can be either larger or smaller than this universal value, which is restored after the averaging. A similar strong dependence of conductance of a clean graphene strip on the boundary conditions was found in Refs. 11 and 22. Our observation of the Aharonov-Bohm flux dependence of the conductivity seems also to be related to the known results on transport properties of disordered wires with chiral symmetry: namely, their dependence on the parity of the number of channels and the staggering in the hopping matrix elements.[92]

V. CONCLUSIONS

To summarize, we have studied the electron transport properties of a disordered graphene layer. We have shown that the nature of disorder is of crucial importance for the behavior of the conductivity. Specifically, it is important (i) whether the individual scatterers are strong or weak and (ii) what the symmetry of the disorder is within the classification of Table I. Our key results are as follows.

(i) *Away from half filling*, the concentration dependence of conductivity is linear (with logarithmic corrections) for strong scatterers (unitary limit), Eq. (65), while it is only logarithmic in the case of weak scatterers (Gaussian disorder), Eq. (52). We have constructed a "phase diagram," Fig. 6, showing which of these types of behavior should be expected for given microscopic parameters of the disorder. We have shown that the physically important case of charged impurities corresponds to the Gaussian-unitary "phase boundary." The linear behavior of the conductivity that we have found for the case of strong scatterers agrees with the experimental findings,[2,3] demonstrating that this kind of disorder is dominant in experimentally studied structures.

(ii) *At half filling*, the conductivity is generically strongly affected by localization effects. However, this is not so for certain special types of disorder symmetry. In particular, we have analyzed in detail the situation when the randomness preserves one of the chiral symmetries of the clean Hamiltonian. We have shown that for this case ("chiral disorder") the conductivity at the Dirac point is of the order of e^2/h. The exact value of the conductivity still depends on the nature of the infrared cutoff, which may depend on the physical setup. We have considered the situation when this cutoff is provided by the level width δ or by the frequency ω; in the first case, the conductivity takes a universal value $4e^2/\pi h$ [see Eqs. (79) and (88)], while in the second case it shows a more complex behavior, Fig. 7.

Whether the chiral disorder may indeed dominate in experimentally relevant structures, explaining the observed value of conductivity $\sim e^2/h$ remains an open question. Alternatively, a value of conductivity $\sim e^2/h$ at the Dirac point can emerge if the dominant disorder does not scatter electrons between the two valleys (see Sec. IV A 5); work in this direction is currently in progress. Further research directions extending our results include, in particular, mesoscopic transport in a phase-coherent disordered sample and effects of interaction and of macroscopic inhomogeneities.

ACKNOWLEDGMENTS

We thank D.I. Diakonov, I.A. Gruzberg, A.W.W. Ludwig, K.S. Novoselov, S.V. Morozov, A.F. Morpurgo, M.A. Skvortsov, and A.G. Yashenkin for valuable discussions. We are also grateful to A.W.W. Ludwig for bringing Ref. 81 to our attention and to S. Ryu, C. Mudry, A. Furusaki, and A.W.W. Ludwig for pointing out Ref. 82 to us. The work was supported by the Center for Functional Nanostructures and the Schwerpunktprogramm "Quanten-Hall-Systeme" of the Deutsche Forschungsgemeinschaft. The work of P.M.O. was supported by the Russian Foundation for Basic Research under Grant No. 04-02-16348 and by the Russian Academy of Sciences under the program "Quantum Macrophysics." The work of I.V.G., conducted as a part of the project "Quantum Transport in Nanostructures" made under the EUROHORCS/ESF EURYI Awards scheme, was supported by funds from the Participating Organizations of EURYI and the EC Sixth Framework Programme and by the Program "Leading Russian Scientific Schools" under Grant No. 2192.2003.2. A.D.M. acknowledges the hospitality of the Kavli Institute for Theoretical Physics at Santa Barbara during the completion of the manuscript and partial support by the National Science Foundation under Grant No. PHY99-07949.

APPENDIX A: ONE-LOOP RG EQUATIONS

The full action containing all possible disorder structures from Table I reads

$$S[\psi] = \int d^2r \Bigg\{ i\bar{\psi}(\varepsilon + iv_0\tau_3\boldsymbol{\sigma}\nabla - i0\Lambda)\psi + \pi v_0^2 \Bigg[\alpha_0(\bar{\psi}\sigma_0\tau_0\psi)^2 + \frac{\alpha_\perp}{2}[(\bar{\psi}\sigma_1\tau_3\psi)^2 + (\bar{\psi}\sigma_2\tau_3\psi)^2] + \alpha_z(\bar{\psi}\sigma_3\tau_0\psi)^2 + \frac{\beta_0}{2}[(\bar{\psi}\sigma_3\tau_1\psi)^2 + (\bar{\psi}\sigma_3\tau_2\psi)^2] + \frac{\beta_\perp}{4}[(\bar{\psi}\sigma_1\tau_1\psi)^2 + (\bar{\psi}\sigma_1\tau_2\psi)^2 + (\bar{\psi}\sigma_2\tau_1\psi)^2 + (\bar{\psi}\sigma_2\tau_2\psi)^2] + \frac{\beta_z}{2}[(\bar{\psi}\sigma_0\tau_1\psi)^2 + (\bar{\psi}\sigma_0\tau_2\psi)^2] + \gamma_0(\bar{\psi}\sigma_0\tau_3\psi)^2 + \frac{\gamma_\perp}{2}[(\bar{\psi}\sigma_1\tau_0\psi)^2 + (\bar{\psi}\sigma_2\tau_0\psi)^2] + \gamma_z(\bar{\psi}\sigma_3\tau_3\psi)^2 \Bigg] \Bigg\}. \tag{A1}$$

A complete set of one-loop perturbative RG equations can be obtained by considering the diagrams of Fig. 5. An impurity line in those diagrams represents a sum of all types of disorder with the proper amplitude and corresponding matrices at the vertices. The RG equations for nine disorder amplitudes [diagrams (b), (c), and (d) in Fig. 5] have the form

$$\frac{d\alpha_0}{d\ln L} = 2\alpha_0(\alpha_0 + \beta_0 + \gamma_0 + \alpha_\perp + \beta_\perp + \gamma_\perp + \alpha_z + \beta_z + \gamma_z) + 2\alpha_\perp\alpha_z + \beta_\perp\beta_z + 2\gamma_\perp\gamma_z, \tag{A2a}$$

$$\frac{d\alpha_\perp}{d\ln L} = 2(2\alpha_0\alpha_z + \beta_0\beta_z + 2\gamma_0\gamma_z), \tag{A2b}$$

$$\frac{d\alpha_z}{d\ln L} = -2\alpha_z(\alpha_0 + \beta_0 + \gamma_0 - \alpha_\perp - \beta_\perp - \gamma_\perp + \alpha_z + \beta_z + \gamma_z) + 2\alpha_0\alpha_\perp + \beta_0\beta_\perp + 2\gamma_0\gamma_\perp, \tag{A2c}$$

$$\frac{d\beta_0}{d\ln L} = 2[\beta_0(\alpha_0 - \gamma_0 + \alpha_\perp + \alpha_z - \gamma_z) + \alpha_\perp\beta_z + \alpha_z\beta_\perp + \beta_\perp\gamma_0], \tag{A2d}$$

$$\frac{d\beta_\perp}{d\ln L} = 4(\alpha_0\beta_z + \alpha_z\beta_0 + \beta_0\gamma_0 + \beta_\perp\gamma_\perp + \beta_z\gamma_z), \tag{A2e}$$

$$\frac{d\beta_z}{d\ln L} = 2[-\beta_z(\alpha_0 - \gamma_0 - \alpha_\perp + \alpha_z - \gamma_z) + \alpha_0\beta_\perp + \alpha_\perp\beta_0 + \beta_\perp\gamma_z], \tag{A2f}$$

$$\frac{d\gamma_0}{d\ln L} = 2\gamma_0(\alpha_0 - \beta_0 + \gamma_0 + \alpha_\perp - \beta_\perp + \gamma_\perp + \alpha_z - \beta_z + \gamma_z) + 2\alpha_\perp\gamma_z + 2\alpha_z\gamma_\perp + \beta_0\beta_\perp, \tag{A2g}$$

$$\frac{d\gamma_\perp}{d\ln L} = 4\alpha_0\gamma_z + 4\alpha_z\gamma_0 + \beta_0^2 + \beta_\perp^2 + \beta_z^2, \tag{A2h}$$

$$\frac{d\gamma_z}{d\ln L} = -2\gamma_z(\alpha_0 - \alpha_\perp + \alpha_z - \beta_0 + \beta_\perp - \beta_z + \gamma_0 - \gamma_\perp + \gamma_z) + 2\alpha_0\gamma_\perp + 2\alpha_\perp\gamma_0 + \beta_\perp\beta_z. \tag{A2i}$$

The RG equation for the energy [diagram (a) in Fig. 5] reads

$$\frac{d\varepsilon}{d\ln L} = \varepsilon(1 + \alpha_0 + \beta_0 + \gamma_0 + \alpha_\perp + \beta_\perp + \gamma_\perp + \alpha_z + \beta_z + \gamma_z). \tag{A2j}$$

For brevity, in this appendix we omit tildes which distinguish running parameters from their initial values in the main text.

In various particular cases, when only some subset of disorder structures is present, these equations reduce to the corresponding form known in the literature. The cases of C_0-chiral ($\alpha_\perp$, $\beta_\perp$, $\gamma_\perp$) and C_z-chiral ($\alpha_\perp$, β_0, β_z, $\gamma_\perp$) disor-

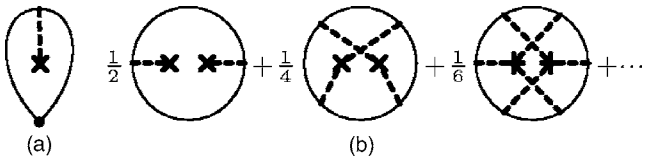

FIG. 8. Diagrams for (a) the first-order correction to the density of states and (b) the second-order correction to the partition function.

der are considered in Sec. IV A. If the disorder is proportional to the τ_3 matrix ($\alpha_\perp$, γ_0, γ_z), the Hamiltonian decouples into two 2×2 blocks, which have the structure of the model with random mass (γ_z), scalar(γ_0), and vector ($\alpha_\perp$) potentials analyzed in Ref. 63. The RG equations for the random mass problem were also given in Refs. 62 and 65, for the random potential in Ref. 64.

If the system possesses a time-reversal invariance (T_0), only the couplings α_0, $\beta_\perp$, β_z, $\gamma_\perp$, and γ_z survive, which is the case considered in Ref. 32. Taking into account the difference between our RG scheme and that of Ref. 32 (where the velocity is renormalized whereas the energy is not), we have checked that the RG equations of Ref. 32 are reproduced from the complete set (A2) if a number of assumptions concerning the hierarchy of the disorder couplings ($\alpha_0 \gg \sqrt{\alpha_0|2\beta_z-\beta_\perp|}, \sqrt{\alpha_0|2\gamma_z-\gamma_\perp|} \gg \beta_z, \beta_\perp, \gamma_z, \gamma_\perp \gg |2\beta_z-\beta_\perp|, |2\gamma_z-\gamma_\perp|$) are made.

APPENDIX B: IMPURITY-INDUCED CORRECTIONS TO THE DENSITY OF STATES IN THE UNITARY LIMIT

In this appendix we calculate the density of states in the presence of infinitely strong impurities (unitary limit) up to the second order in their concentration n_{imp}. The contribution of the first order in n_{imp} is determined by the diagram [Fig. 8(a)] containing a single T matrix[93]

$$\delta\rho^{(1)}(\varepsilon) = -\frac{4}{\pi}\,\mathrm{Im}\,\frac{\eta\Delta^2}{2[\varepsilon\ln(\Delta/|\varepsilon|)+i\pi|\varepsilon|/2]}\int\frac{d^2k}{(2\pi)^2} \times\frac{\varepsilon^2+v_0^2k^2}{[(\varepsilon+i0)^2-v_0^2k^2]^2} = -\frac{\eta\Delta^2}{2\pi v_0^2|\varepsilon|\ln^2(\Delta/|\varepsilon|)}. \tag{B1}$$

This result corresponds to Eq. (59). Obviously, the first-order contribution to the density of states is correctly taken into account by the self-consistent unitary approximation.

The problem becomes more complicated when one looks for the second-order contribution. The calculations are greatly simplified in the coordinate representation and for Matsubara energies. The Green function and the T matrix have the form

$$G_0(i\epsilon,\mathbf{r}) = -\frac{i\epsilon}{2\pi v_0^2}\left[K_0\left(\frac{\epsilon r}{v_0}\right)+\tau_3\boldsymbol{\sigma}\hat{\mathbf{r}}K_1\left(\frac{\epsilon r}{v_0}\right)\right], \tag{B2}$$

$$T(i\epsilon) = \frac{2\pi v_0^2}{ib\epsilon\ln(\Delta/\epsilon)}, \quad b=\begin{cases}1, & \text{long range},\\ 4, & \text{short range}.\end{cases} \tag{B3}$$

The T matrix has different values in the limits of long- and short-range potential disorder. Equation (B2) for the Green function applies for not too short distances. One has to cut the real-space integrals at $r\sim v_0/\Delta$.

We are going to express the density of states in terms of the partition function per unit area. The contribution to this quantity of the second order in η is given by the diagrams in Fig. 8(b),

$$Z_2(i\epsilon) = n_{\mathrm{imp}}^2\mathrm{Tr}\sum_{m=1}^{\infty}\frac{T^{2m}}{2m}\int d^2r[G(r)G(-r)]^m = -2n_{\mathrm{imp}}^2\int d^2r\ln\left\{1-\left(\frac{T\epsilon}{2\pi v_0^2}\right)^2 \times\left[K_1^2\left(\frac{\epsilon r}{v_0}\right)-K_0^2\left(\frac{\epsilon r}{v_0}\right)\right]\right\}. \tag{B4}$$

The correction to the density of states can be represented in the form

$$\delta\rho^{(2)}(\varepsilon) = -\frac{1}{\pi}\,\mathrm{Im}\left.\frac{dZ_2}{d(i\epsilon)}\right|_{i\epsilon\to\varepsilon+i0} = 8v_0^2n_{\mathrm{imp}}^2 \times\mathrm{Im}\left[\frac{i}{\epsilon^3}\int\frac{dz\,zK_1^2(z)}{b^2\ln^2(\Delta/\epsilon)+K_1^2(z)-K_0^2(z)}\right]_{i\epsilon\to\varepsilon+i0}. \tag{B5}$$

For $\mathcal{L}=b\ln(\Delta/\epsilon)\gg 1$ we split the integral over z into two parts and observe that it is dominated by the domain $z>1/\mathcal{L}$:

$$\int_0^\infty\frac{dz\,zK_1^2(z)}{\mathcal{L}^2+K_1^2(z)-K_0^2(z)} \simeq \int_0^{1/\mathcal{L}}dz\,z+\frac{1}{\mathcal{L}^2}\int_{1/\mathcal{L}}^\infty dz\,zK_1^2(z) \simeq \frac{\ln\mathcal{L}}{\mathcal{L}^2}. \tag{B6}$$

Substituting this in Eq. (B5) and performing the analytical continuation, we finally arrive at

$$\delta\rho_2(\varepsilon) = 8v_0^2n_{\mathrm{imp}}^2\mathrm{Im}\left[\frac{i}{\epsilon^3}\frac{\ln\ln(\Delta/\epsilon)}{b^2\ln^2(\Delta/\epsilon)}\right]_{i\epsilon\to\varepsilon+i0} = -\frac{8\pi v_0^2n_{\mathrm{imp}}^2}{b^2|\varepsilon|^3}\frac{\ln\ln(\Delta/|\varepsilon|)}{\ln^3(\Delta/|\varepsilon|)} = -2\rho(\varepsilon)\alpha_U^2(\varepsilon)\ln\frac{\Delta}{|\varepsilon|}\ln\ln\frac{\Delta}{|\varepsilon|}, \tag{B7}$$

where $\alpha_U(\varepsilon)$ is determined by Eq. (60).

*Also at A.F. Ioffe Physico-Technical Institute, 194021 St. Petersburg, Russia.
†Also at Petersburg Nuclear Physics Institute, 188350 St. Petersburg, Russia.
[1] K. S. Novoselov, A. K. Geim, S. V. Morozov, D. Jiang, Y. Zhang, S. V. Dubonos, I. V. Grigorieva, and A. A. Firsov, Science **306**, 666 (2004).
[2] K. S. Novoselov, A. K. Geim, S. V. Morozov, D. Jiang, M. I. Katsnelson, I. V. Grigorieva, S. V. Dubonos, and A. A. Firsov, Nature (London) **438**, 197 (2005).
[3] Y. Zhang, Y.-W. Tan, H. L. Stormer, and P. Kim, Nature (London) **438**, 201 (2005).
[4] K. S. Novoselov, E. McCann, S. V. Morozov, V. I. Falko, M. I. Katsnelson, U. Zeitler, D. Jiang, F. Schedin, and A. K. Geim, Nat. Phys. **2**, 177 (2006).
[5] S. V. Morozov, K. S. Novoselov, M. I. Katsnelson, F. Schedin, L. A. Ponomarenko, D. Jiang, and A. K. Geim, Phys. Rev. Lett. **97**, 016801 (2006).
[6] Y. Zhang, Z. Jiang, J. P. Small, M. S. Purewal, Y.-W. Tan, M. Fazlollahi, J. D. Chudow, J. A. Jaszczak, H. L. Stormer, and P. Kim, Phys. Rev. Lett. **96**, 136806 (2006).
[7] E. McCann and V. I. Fal'ko, Phys. Rev. B **71**, 085415 (2005).
[8] E. McCann and V. I. Fal'ko, Phys. Rev. Lett. **96**, 086805 (2006).
[9] V. P. Gusynin and S. G. Sharapov, Phys. Rev. Lett. **95**, 146801 (2005); Phys. Rev. B **73**, 245411 (2006); V. P. Gusynin, S. G. Sharapov, and J. P. Carbotte, Phys. Rev. Lett. **96**, 256802 (2006); V. P. Gusynin, V. A. Miransky, S. G. Sharapov, and I. A. Shovkovy, Phys. Rev. B **74**, 195429 (2006); V. P. Gusynin, S. G. Sharapov, and J. P. Carbotte, cond-mat/0607727 (unpublished).
[10] C. L. Kane and E. J. Mele, Phys. Rev. Lett. **95**, 226801 (2005).
[11] M. I. Katsnelson, Eur. Phys. J. B **51**, 157 (2006); **52**, 151 (2006).
[12] M. I. Katsnelson, K. S. Novoselov, and A. K. Geim, Nat. Phys. **2**, 620 (2006).
[13] V. M. Pereira, F. Guinea, J. M. B. Lopes dos Santos, N. M. R. Peres, and A. H. Castro Neto, Phys. Rev. Lett. **96**, 036801 (2006); N. M. R. Peres, F. Guinea, and A. H. Castro Neto, Phys. Rev. B **72**, 174406 (2005); **73**, 125411 (2006); N. M. R. Peres, A. H. Castro Neto, and F. Guinea, *ibid.* **73**, 195411 (2006); **73**, 241403 (2006); A. H. Castro Neto, F. Guinea, and N. M. R. Peres, *ibid.* **73**, 205408 (2006); F. Guinea, A. H. Castro Neto, and N. M. R. Peres, *ibid.* **73**, 245426 (2006).
[14] A. F. Morpurgo and F. Guinea, Phys. Rev. Lett. **97**, 196804 (2006).
[15] M. Koshino and T. Ando, Phys. Rev. B **73**, 245403 (2006).
[16] T. Ando, J. Phys. Soc. Jpn. **75**, 074716 (2006).
[17] L. Brey and H. A. Fertig, Phys. Rev. B **73**, 195408 (2006); **73**, 235411 (2006).
[18] D. A. Abanin, P. A. Lee, and L. S. Levitov, Phys. Rev. Lett. **96**, 176803 (2006).
[19] Yu. G. Pogorelov, cond-mat/0603327 (unpublished).
[20] V. V. Cheianov and V. I. Fal'ko, Phys. Rev. B **74**, 041403(R) (2006).
[21] D. V. Khveshchenko, Phys. Rev. Lett. **97**, 036802 (2006); Phys. Rev. B **74**, 161402(R) (2006).
[22] J. Tworzydlo, B. Trauzettel, M. Titov, A. Rycerz, and C. W. J. Beenakker, Phys. Rev. Lett. **96**, 246802 (2006).
[23] M. Titov and C. W. J. Beenakker, Phys. Rev. B **74**, 041401(R) (2006).
[24] C. W. J. Beenakker, Phys. Rev. Lett. **97**, 067007 (2006).
[25] M. S. Foster and A. W. W. Ludwig, Phys. Rev. B **73**, 155104 (2006).
[26] E. McCann, K. Kechedzhi, V. I. Fal'ko, H. Suzuura, T. Ando, and B. L. Altshuler, Phys. Rev. Lett. **97**, 146805 (2006).
[27] Yu. V. Skrypnyk and V. M. Loktev, Phys. Rev. B **73**, 241402(R) (2006).
[28] H. Kumazaki and D. S. Hirashima, J. Phys. Soc. Jpn. **75**, 53707 (2006).
[29] K. Nomura and A. H. MacDonald, Phys. Rev. Lett. **96**, 256602 (2006).
[30] K. Nomura and A. H. MacDonald, cond-mat/0606589 (unpublished).
[31] L. A. Falkovsky and A. A. Varlamov, cond-mat/0606800 (unpublished).
[32] I. L. Aleiner and K. B. Efetov, Phys. Rev. Lett. **97**, 236801 (2006).
[33] A. Altland, Phys. Rev. Lett. **97**, 236802 (2006).
[34] V. Cheianov and V. I. Fal'ko, Phys. Rev. Lett. **97**, 226801 (2006).
[35] E. McCann, Phys. Rev. B **74**, 161403(R) (2006).
[36] N. A. Sinitsyn, A. H. MacDonald, T. Jungwirth, V. K. Dugaev, and J. Sinova, cond-mat/0608682 (unpublished).
[37] I. A. Luk'yanchuk and Y. Kopelevich, cond-mat/0609037 (unpublished).
[38] I. Snyman and C. W. J. Beenakker, cond-mat/0609243 (unpublished).
[39] H. P. Dahal, Y. N. Joglekar, K. S. Bedell, and A. V. Balatsky, cond-mat/0609440 (unpublished).
[40] T. O. Wehling, A. V. Balatsky, M. I. Katsnelson, A. I. Lichtenstein, K. Scharnberg, and R. Wiesendanger, cond-mat/0609503 (unpublished).
[41] P. R. Wallace, Phys. Rev. **71**, 622 (1947).
[42] T. Ando, J. Phys. Soc. Jpn. **74**, 777 (2005).
[43] N. H. Shon and T. Ando, J. Phys. Soc. Jpn. **67**, 2421 (1998).
[44] J. González, F. Guinea, and M. A. H. Vozmediano, Phys. Rev. B **63**, 134421 (2001); T. Stauber, F. Guinea, and M. A. H. Vozmediano, *ibid.* **71**, 041406(R) (2005); M. A. H. Vozmediano, F. Guinea, and M. P. López-Sancho, J. Phys. Chem. Solids **67**, 562 (2006).
[45] S. Guruswamy, A. LeClair, and A. W. W. Ludwig, Nucl. Phys. B **583**, 475 (2000).
[46] Since Ref. 32 uses a representation different from Eq. (1) and thus a form of the bare Dirac Hamiltonian different from Eq. (2), the identification of the types of disorder requires the corresponding unitary transformation.
[47] For applications of the SCTMA to systems of disordered Dirac fermions in the context of *d*-wave superconductors, see, e.g., Refs. 48–55.
[48] P. J. Hirschfeld, P. Wölfle, and D. Einzel, Phys. Rev. B **37**, 83 (1988).
[49] A. C. Durst and P. A. Lee, Phys. Rev. B **62**, 1270 (2000).
[50] C. Chamon and C. Mudry, Phys. Rev. B **63**, 100503(R) (2001).
[51] A. G. Yashenkin, W. A. Atkinson, I. V. Gornyi, P. J. Hirschfeld, and D. V. Khveshchenko, Phys. Rev. Lett. **86**, 5982 (2001).
[52] P. J. Hirschfeld and W. A. Atkinson, J. Low Temp. Phys. **126**, 881 (2002).
[53] A. Altland, Phys. Rev. B **65**, 104525 (2002).
[54] V. M. Loktev and Yu. G. Pogorelov, Phys. Lett. A **320**, 307 (2004); cond-mat/0308427 (unpublished).
[55] A. V. Balatsky, I. Vekhter, and J.-X. Zhu, Rev. Mod. Phys. **78**, 373 (2006).

[56] Y. Zheng and T. Ando, Phys. Rev. B **65**, 245420 (2002); T. Ando, Y. Zheng, and H. Suzuura, J. Phys. Soc. Jpn. **71**, 1318 (2002).
[57] In the context of Dirac fermions in disordered superconductors and degenerate semiconductors the SCBA scheme was developed in Refs. 58–60.
[58] L. P. Gorkov and P. A. Kalugin, Pis'ma Zh. Eksp. Teor. Fiz. **41**, 208 (1985) [JETP Lett. **41**, 253 (1985)].
[59] E. Fradkin, Phys. Rev. B **33**, 3257 (1986); **33**, 3263 (1986).
[60] P. A. Lee, Phys. Rev. Lett. **71**, 1887 (1993).
[61] In fact, a careful analysis of the SCBA equation yields $\alpha\Gamma_0 = \Gamma_0/\ln(\Delta/\Gamma_0)$ for the position of the crossover between the high- and the low-energy asymptotics in Eq. (34). For simplicity, we omit such logarithmic prefactors in the expressions for the boundary between the high- and the low-energy regimes in Eq. (34) and below.
[62] V. S. Dotsenko and V. S. Dotsenko, Adv. Phys. **32**, 129 (1983).
[63] A. W. W. Ludwig, M. P. A. Fisher, R. Shankar, and G. Grinstein, Phys. Rev. B **50**, 7526 (1994).
[64] A. A. Nersesyan, A. M. Tsvelik, and F. Wenger, Phys. Rev. Lett. **72**, 2628 (1994); Nucl. Phys. B **438**, 561 (1995).
[65] M. Bocquet, D. Serban, and M. R. Zirnbauer, Nucl. Phys. B **578**, 628 (2000).
[66] A. Altland, B. D. Simons, and M. R. Zirnbauer, Phys. Rep. **359**, 283 (2002).
[67] It is worth mentioning that the current operator $ev_0\bar{\psi}\tau_3\boldsymbol{\sigma}\psi$ is not renormalized within the considered ultraviolet (ballistic) RG, apart from its engineering dimension. Indeed, the retarded-retarded current operator $ev_0\bar{\psi}^R\tau_3\boldsymbol{\sigma}\psi^R$ is related to the kinetic term $iv_0\bar{\psi}\tau_3\boldsymbol{\sigma}\nabla\psi$ by virtue of gauge invariance and thus does not acquire any anomalous scaling. Further, since the ultraviolet RG works identically for RR and RA operators, this statement applies to the latter as well.
[68] P. Wölfle and R. N. Bhatt, Phys. Rev. B **30**, 3542 (1984); R. N. Bhatt, P. Wölfle, and T. V. Ramakrishnan, *ibid.* **32**, 569 (1985).
[69] Another feature of such a crossover—also not observed experimentally—would be the asymmetric energy dependence of the density of states (Ref. 19) and conductivity in the realistic case of positive impurity potential. In the Born limit, the chemical potential is shifted by $\delta\mu = n_{\mathrm{imp}}U \sim \Delta(\alpha\eta)^{1/2}$, whereas in the unitary case this shift vanishes. Also, the density of states would exhibit a resonant structure related to emergence of bound states (Refs. 19, 40, and 55).
[70] R. Gade, Nucl. Phys. B **398**, 499 (1993).
[71] The second term in the denominator of Eq. (67) (polarization function) is written in the Thomas-Fermi approximation valid for $q \lesssim \varepsilon/v_0$; for larger momenta, it will be suppressed by a factor $\varepsilon/qv_0 \ll 1$. This is, however, not important, since for such q the first term (bare interaction) dominates anyway.
[72] M. I. Katsnelson, Phys. Rev. B **74**, 201401(R) (2006).
[73] The Thomas-Fermi approach implies the locality of the nonlinear response function $\Pi_3(\mathbf{r},\mathbf{r}',\mathbf{r}'') = (\partial^2 n/\partial\mu^2)\delta(\mathbf{r}-\mathbf{r}')\delta(\mathbf{r}-\mathbf{r}'')$ [in the momentum representation $\tilde{\Pi}_3(\mathbf{q},\mathbf{q}',\mathbf{q}'') = \partial^2 n/\partial\mu^2\,\delta(\mathbf{q}+\mathbf{q}'+\mathbf{q}'')$] represented by a three-leg fermionic loop. This form is valid only on spatial scales much larger than the Fermi wavelength. In Ref. 72, the Thomas-Fermi approximation has been applied to the scales shorter than the Fermi wavelength ($a < \mathbf{r}', \mathbf{r}'' < \lambda_\mu$)—i.e., for $\mu \ll qv_0 \ll \Delta$. On such scales the nonlinear response function Π_3 is nonlocal in space (in momentum representation it is suppressed by $1/q^2$) which eliminates all the ultraviolet logarithmic singularities.
[74] T. Ando, T. Nakanishi, and R. Saito, J. Phys. Soc. Jpn. **67**, 2857 (1998); H. Suzuura and T. Ando, Phys. Rev. Lett. **89**, 266603 (2002).
[75] R. Gade and F. Wegner, Nucl. Phys. B **360**, 213 (1991).
[76] In Refs. 45 and 70 the function $f(\varepsilon)$ was found to be of the form $f(\varepsilon) \sim \exp\{-c|\ln\varepsilon|^x\}$ with $x=1/2$; later works (Refs. 77 and 78) corrected the value of x to $x=2/3$.
[77] O. Motrunich, K. Damle, and D. A. Huse, Phys. Rev. B **65**, 064206 (2001).
[78] C. Mudry, S. Ryu, and A. Furusaki, Phys. Rev. B **67**, 064202 (2003).
[79] M. R. Zirnbauer, J. Math. Phys. **37**, 4986 (1996).
[80] A. Altland and M. R. Zirnbauer, Phys. Rev. B **55**, 1142 (1997).
[81] D. Bernard and A. LeClair, J. Phys. A **35**, 2555 (2002).
[82] A. M. Tsvelik, Phys. Rev. B **51**, 9449 (1995).
[83] P. Fendley and R. M. Konik, Phys. Rev. B **62**, 9359 (2000).
[84] A. W. W. Ludwig, cond-mat/0012189 (unpublished).
[85] J. Schwinger, Phys. Rev. **128**, 2425 (1962).
[86] M. E. Peskin and D. V. Schroeder, *An Introduction to Quantum Field Theory*, Addison-Wesley Advanced Book Program (Westview Press, Boulder, 1995).
[87] S. Hikami, M. Shirai, and F. Wegner, Nucl. Phys. B **408**, 415 (1993).
[88] K. B. Efetov, *Supersymmetry in Disorder and Chaos* (Cambridge University Press, Cambridge, England, 1996).
[89] Y. Hatsugai, X.-G. Wen, and M. Kohmoto, Phys. Rev. B **56**, 1061 (1997).
[90] S. Ryu, C. Mudry, A. Furusaki, and A. W. W. Ludwig, cond-mat/0610598 (unpublished).
[91] M. S. Foster and A. W. W. Ludwig, Phys. Rev. B **74**, 241102 (2006).
[92] P. W. Brouwer, C. Mudry, B. D. Simons, and A. Altland, Phys. Rev. Lett. **81**, 862 (1998).
[93] Equation (B1) differs from the result of C. Pepin and P. A. Lee, Phys. Rev. B **63**, 054502 (2001), by a sign. We also disagree with the statement made in this work that $\delta\rho^{(1)}(\varepsilon)$ governs the low-energy asymptotics of ρ.